Eur. Phys. J. A **9**, 73–94 (2000)

THE EUROPEAN PHYSICAL JOURNAL A

A relativistic quark model for mesons with an instanton-induced interaction

M. Koll[a], R. Ricken, D. Merten, B.C. Metsch, and H.R. Petry

Institut für Theoretische Kernphysik, Nußallee 14-16, D-53115 Bonn, Germany

Received: 28 August 2000
Communicated by V.V. Anisovich

Abstract. We present new results of a relativistic quark model based on the Bethe-Salpeter equation in its instantaneous approximation. Assuming a linearly rising confinement potential with an appropriate spinorial structure in Dirac space and adopting a residual interaction based on instanton effects, we can compute masses of the light mesons up to highest observed angular momenta with a natural solution of the $U_A(1)$ problem. The calculated ground states masses and the radial excitations describe the experimental results well. In this paper, we will also discuss our results concerning numerous meson decay properties. For processes like $\pi^+/K^+ \to e^+\nu_e\gamma$ and $0^- \to \gamma\gamma$ at various photon virtualities, we find a good agreement with experimental data. We will also comment on the form factors of the $K_{\ell 3}$ decay and on the decay constants of the π, K and η mesons. For the sake of completeness, we will furthermore present the electromagnetic form factors of the charged π and K mesons as well as a comparison of the radiative meson decay widths with the most recent experimental data.

PACS. 11.10.St Bound and unstable states; Bethe-Salpeter equations – 12.39.Ki Relativistic quark model – 12.40.Yx Hadron mass models and calculations – 14.65.Bt Light quarks

1 Introduction

After years of research on the problem of bound states in QCD, there are still lots of open questions. Since it is not possible to apply a perturbative treatment of QCD in the low-energy region around $\approx 1\,\mathrm{GeV}$, one has to rely on effective theoretical descriptions of hadrons. Integrating out the quark degrees of freedom leads to approaches such as Chiral Perturbation Theory or the Nambu–Jona-Lasinio model, but these ideas fail in the description of higher-lying resonances and radial excitations. These states can be described (even in a non-relativistic treatment at least qualitatively) by models including quark confinement (see, *e.g.*, [1]).

In this paper, we discuss some new results on light meson spectra and decays in the framework of a relativistic quark model that has been presented in some previous publications (see [2–10]). In particular, we want to update our results on mass spectra and electroweak decay properties, consistently calculated with a parameter set that gives a global description of the complete meson spectrum. At the same time, we shall discuss new results from an alternative description of confinement. Our model is based on the Bethe-Salpeter equation in its instantaneous approximation and provides an excellent description of the masses of the complete meson spectrum including highest angular momenta and radial excitations. We will study these spectra and compare our results not only with the latest Particle Data Group (PDG) compilation [19] but also with alternative new interpretations of meson resonances as $q\bar{q}$ states or exotics. The model that is presented here can also be applied to various meson decay processes and shows a good overall agreement compared to the experimental data. We will investigate the pseudoscalar decay constants and their relation to the decays of $J^\pi = 0^-$ mesons into two photons at some selected photon virtualities. The electromagnetic structure of the charged π and K mesons will be discussed by presenting their form factors, calculated in the parameter sets used in this paper. Since we want to update our former publications, we will also briefly resume the status of the electromagnetic decay widths in our model. Furthermore, we compute form factors for the processes $\pi^+/K^+ \to e^+\nu_e\gamma$ and $K^+ \to \pi^0 e^+\nu_e$ (the so-called $K_{\ell 3}$ decay).

We have organized this article as follows: section 2 gives a synopsis of our model and introduces the potentials adopted in the subsequent evaluations. Section 3 is devoted to a discussion of the parameters and their effects on the resulting meson spectra. We will present calculations on various decay processes in section 4 before we conclude with summarizing remarks in section 5.

[a] e-mail: koll@itkp.uni-bonn.de

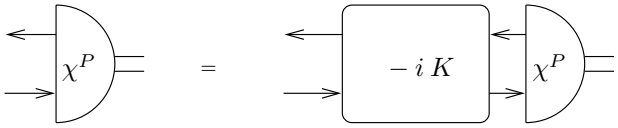

Fig. 1. The Bethe-Salpeter equation for $q\bar{q}$ bound states in a graphical notation.

2 A relativistic quark model on the basis of the instantaneous Bethe-Salpeter equation

Our results will be presented in the framework of a relativistic quark model based on the Bethe-Salpeter (BS) equation (see [11]) for a $q\bar{q}$ bound state of four-momentum P and mass M with $M^2 = P^2$:

$$\chi^P(p) = -i\, S_1^F(\eta_1 P + p) \times \left[\int \frac{\mathrm{d}^4p'}{(2\pi)^4} K(P;p,p')\chi^P(p')\right] S_2^F(-\eta_2 P + p), \quad (1)$$

see fig. 1 for a diagrammatic representation of this equation. Here, $S_i^F(\pm\eta_i P + p)$ denotes the full quark propagator where $i = 1$ indicates the quark, $i = 2$ the antiquark and p is the relative momentum between quark and antiquark. The coefficients η_i satisfying the condition $\eta_1 + \eta_2 = 1$ fix a special choice of coordinates; in the following considerations, we will set $\eta_1 = \eta_2 = \frac{1}{2}$ for the sake of simplicity.

The BS amplitude χ^P is defined in coordinate space as the time-ordered product of two (anti-)quark field operators:

$$\chi^P_{\alpha\beta}(x_1,x_2) := \left\langle\, 0 \,\left|T\,\psi^1_\alpha(x_1)\bar{\psi}^2_\beta(x_2)\right|\, P\,\right\rangle = e^{-iP\cdot\frac{x_1+x_2}{2}} \int \frac{\mathrm{d}^4p}{(2\pi)^4} e^{-ip\cdot(x_1-x_2)} \chi^P_{\alpha\beta}(p), \quad (2)$$

where α and β stand for Dirac, flavour and colour indices. The function $K(P;p,p')$ in the BS equation represents the four-dimensional irreducible kernel including all interactions between the $q\bar{q}$ pair. Neither the full propagator $S_i^F(\pm P/2 + p)$ nor the interaction kernel $K(P;p,p')$ are sufficiently well known and have to be fixed by appropriate phenomenological assumptions. In our model, we adopt the so-called instantaneous approximation for the kernel that was originally proposed by Salpeter (see [12]). It can be formulated covariantly via

$$K(P;p,p') = V(p_\perp, p'_\perp)\,, \quad (3)$$

where we have introduced components of the relative momentum $p = p_\parallel + p_\perp$ parallel and perpendicular to the meson momentum P by

$$p_\parallel := \frac{p\cdot P}{\sqrt{P^2}} \quad \text{and} \quad p_\perp := p - \frac{p\cdot P}{\sqrt{P^2}}\,. \quad (4)$$

In the rest frame of the meson where $P = (M,\vec{0})$, we find $p_\parallel = (p^0,\vec{0})$ and $p_\perp = (0,\vec{p})$ yielding finally

$$K(P;p,p')|_{P=(M,\vec{0})} = V(\vec{p},\vec{p}') \quad (5)$$

for the instantaneous interaction kernel. This formally covariant formulation allows to transform any solution χ^P of the BS equation that is found in the meson rest frame with $P = (M,\vec{0})$ into a solution for non-vanishing meson momenta. This is an important point since it turned out to be crucial for a satisfying description of, *e.g.*, the pion form factor already at moderate Q^2 that indeed the correct Lorentz boost is applied to the BS amplitudes of the π meson (see [5]).

The second model assumption states that the quark propagators in the BS equation can suitably be approximated by free propagators according to

$$S_i^F(p) \approx i\,\frac{\not{p} + m_i}{p^2 - m_i^2} = i\left(\frac{\Lambda_i^+(\vec{p})}{p^0 - \omega_i + i\varepsilon} + \frac{\Lambda_i^-(\vec{p})}{p^0 + \omega_i - i\varepsilon}\right)\gamma^0\,, \quad (6)$$

where m_i is the effective constituent mass (either for *non-strange* or *strange* flavours in the case of light mesons) with $\omega_i = \sqrt{\vec{p}^{\,2} + m_i^2}$ the energy of the (anti-)quark i. The projectors

$$\Lambda_i^\pm(\vec{p}) := \frac{1}{2} \pm \frac{H_i(\vec{p})}{2\omega_i}\,, \quad (7)$$

with the standard single-particle Dirac Hamiltonian $H_i(\vec{p}) = \gamma^0(\vec{\gamma}\vec{p} + m_i)$ distinguish states of positive and negative energy of (anti-)quark i.

With these assumptions and since the p^0-dependence of the interaction kernel vanishes in the instantaneous approximation, the p^0 integration of eq. (1) in the meson's rest frame can be performed analytically via the residue theorem thus leading to the so-called Salpeter equation (see[12]):

$$\Phi(\vec{p}) = +\,\Lambda_1^-(\vec{p})\gamma^0\left[\int \frac{\mathrm{d}^3p'}{(2\pi)^3}\frac{V(\vec{p},\vec{p}')\Phi(\vec{p}')}{M + \omega_1 + \omega_2}\right]\gamma^0\Lambda_2^+(-\vec{p}) - \Lambda_1^+(\vec{p})\gamma^0\left[\int \frac{\mathrm{d}^3p'}{(2\pi)^3}\frac{V(\vec{p},\vec{p}')\Phi(\vec{p}')}{M - \omega_1 - \omega_2}\right]\gamma^0\Lambda_2^-(-\vec{p}). \quad (8)$$

Here, the Salpeter amplitude defined by $\Phi(\vec{p}) := \int \frac{\mathrm{d}p^0}{2\pi}\,\chi^P(p^0,\vec{p})\big|_{P=(M,\vec{0})}$ depends only on the space-like components of the meson's relative momentum p.

In previous papers, it has been shown how to formulate the Salpeter equation as an eigenvalue problem

$$(\mathcal{H}\Psi)(\vec{p}) = M\Psi(\vec{p})\,, \quad (9)$$

with $\Psi(\vec{p}) := \Phi(\vec{p})\gamma^0$ and M the mass of the the $q\bar{q}$ bound state considered. For more details, we refer the reader to [2] and [3] where also the numerical treatment of this eigenvalue equation is discussed.

With an adequate potential ansatz, it is thus possible to calculate meson mass spectra on the basis of the Salpeter equation. Since we wish a proper description not only of the Regge trajectories $M^2 \propto J$ but also of the intriguing scalar sector and the characteristic pseudoscalar splittings, we do not consider potentials derived

Table 1. The parameters of the confinement force, the 't Hooft interaction and the constituent quark masses in the models $\mathcal{A}$ and $\mathcal{B}$.

	Parameter	Model $\mathcal{A}$	Model $\mathcal{B}$
't Hooft interaction	g [GeV^{-2}]	1.73	1.62
	g' [GeV^{-2}]	1.54	1.35
	Λ_{III} [fm]	0.30	0.42
Constituent quark masses	m_n [MeV]	306	380
	m_s [MeV]	503	550
Confinement parameters	a_c [MeV]	–1751	–1135
	b_c [MeV/fm]	2076	1300
Spin structure	$\Gamma \otimes \Gamma$	$\frac{1}{2}(\mathbb{1} \otimes \mathbb{1} - \gamma_0 \otimes \gamma_0)$	$\frac{1}{2}(\mathbb{1} \otimes \mathbb{1} - \gamma_\mu \otimes \gamma^\mu - \gamma_5 \otimes \gamma_5)$

from (flavour-independent) one-gluon–exchange diagrams but we adopt the following to describe the underlying quark dynamics:

– A linear confinement potential with $\mathcal{V}_C(x) = a_c + b_c \cdot x$ in coordinate space and an appropriate spinorial structure $\Gamma \otimes \Gamma$ in Dirac space acting like

$$\int \frac{\mathrm{d}^3p'}{(2\pi)^3}\, V_C\,(\vec{p},\vec{p}\,')\Phi(\vec{p}\,') = \int \frac{\mathrm{d}^3p'}{(2\pi)^3}\tilde{\mathcal{V}}_C\left((\vec{p}-\vec{p}\,')^2\right)\Gamma\Phi(\vec{p}\,')\Gamma \quad (10)$$

in momentum space. The confinement offset a_c and its slope b_c are free parameters of our model. Various spin dependencies have been investigated. Below, we will discuss two variants that both yield a stable solution of the Salpeter equation and at the same time reproduce the states on the Regge trajectories correctly.

– A flavour-dependent two-body force from an instanton-induced interaction (abbr.: III), following an idea of 't Hooft (see [13,3] and references therein):

$$\int \frac{\mathrm{d}^3p'}{(2\pi)^3}V_{\mathrm{III}}(\vec{p},\vec{p}\,')\Phi(\vec{p}\,') = 4G(g,g')\int \frac{\mathrm{d}^3p'}{(2\pi)^3}\mathcal{R}_\Lambda\,(\vec{p},\vec{p}\,') \times\Big(\mathbb{1}\mathrm{tr}\big[\Phi(\vec{p}\,')\big] + \gamma_5\mathrm{tr}\big[\Phi(\vec{p}\,')\gamma_5\big]\Big). \quad (11)$$

Here, $\mathcal{R}_\Lambda$ represents a regularizing function and $G(g,g')$ is a flavour matrix, *i.e.* a summation over flavour indices is understood. We treat the coupling strengths g (*non-strange* sector), g' (*non-strange/strange* sector) and the finite effective range $\Lambda = \Lambda_{\mathrm{III}}$ as free parameters.

The latter feature enables us to describe properly the π-K-η-η' mass splittings; without an explicit flavour-dependent residual interaction, their masses would be partly degenerate.

Let us finally introduce the meson-quark-antiquark vertex function Γ^P (or the amputated BS amplitude) which is defined by

$$\Gamma^P(p) := \left[S_1^F\left(\frac{P}{2}+p\right)\right]^{-1}\,\chi^P(p)\,\left[S_2^F\left(-\frac{P}{2}+p\right)\right]^{-1}. \quad (12)$$

It depends only on variables $p_\perp$ of a three-dimensional subspace and therefore reduces in the rest frame of the meson to

$$\Gamma^P(p)\big|_{P=(M,\vec{0})} = -i\int\frac{\mathrm{d}^3p'}{(2\pi)^3}V(\vec{p},\vec{p}\,')\Phi(\vec{p}\,') =: \Gamma(\vec{p}\,), \quad (13)$$

which can be seen by inserting $\Gamma^P(p)$ in the BS equation with an instantaneous interaction kernel. After simultaneously computing the mass spectra and the associated Salpeter amplitudes with eq. (9), it is therefore possible to reconstruct the BS amplitudes χ^P in the meson's rest frame with eqs. (12) and (13).

It has been shown in [5] that — for a pure boost defined by $P = \Lambda_P\tilde{P}$, with $\tilde{P} = (M,\vec{0})$ — the rest frame BS amplitude $\chi^{\tilde{P}}$ is linked via $\chi^P(p) = S_{\Lambda_P}\chi^{\tilde{P}}(\Lambda_P^{-1}p)S_{\Lambda_P}^{-1}$ to the amplitude χ^P for any on-shell momentum P ($P^2 = M^2$) of the $q\bar{q}$ bound state considered; here, S_{Λ_P} is a matrix acting on the spinor indices of χ^P that obeys $S_{\Lambda_P}\gamma_\mu S_{\Lambda_P}^{-1} = (\Lambda_P)_\mu{}^\nu\gamma_\nu$.

A similar relation holds for the vertex function Γ^P so that we regard our model as fully relativistic (and not only "relativized") as it fulfills the general prescriptions for Lorentz boosts. This can be seen as a consequence of the covariant formulation of our ansatz which is in fact possible in spite of the use of the instantaneous kernels in the BS equation as has been shown above.

3 Parameters and mass spectra

As discussed in the previous section, the relativistic quark model presented here contains some free parameters: the effective constituent quark masses m_n and m_s, the confinement parameters a_c and b_c (together with an appropriate

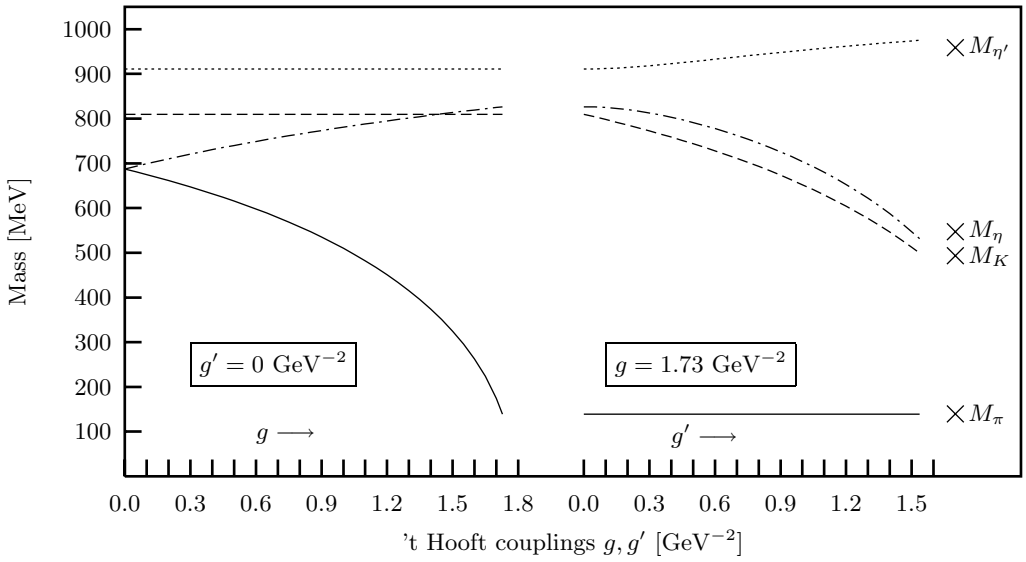

Fig. 2. The effect of 't Hooft's instanton-induced interaction on the masses of the pseudoscalar mesons with the parameters of model $\mathcal{A}$. Solid line: M_π; dashed line: M_K; dashed-dotted line: M_η; dotted line: $M_{\eta'}$; crosses denote the experimental masses from the Particle Data Group (see [19]).

Table 2. The coefficients for the *non-strange/strange* mixing in the η and η' mesons according to eq. (16), calculated with the parameters of the models $\mathcal{A}$ and $\mathcal{B}$. The Mark III group used an unconstrained fit in the evaluation of the coefficients while $X^2_\mathcal{M} + Y^2_\mathcal{M} = 1$ ($\mathcal{M} = \eta, \eta'$) was demanded in the DM2 analysis. Note that the results of refs. [22] and [24] are found in the so-called one-angle mixing scheme of eq. (17) where by definition $|X_\eta| = |Y_{\eta'}|$ and $|Y_\eta| = |X_{\eta'}|$ is fixed.

Coefficient	Model $\mathcal{A}$	Model $\mathcal{B}$	Mark III [25]	DM2 [26]	Ref. [22]	Ref. [24]
$\lvert X_\eta \rvert$	0.68	0.74	0.67 ± 0.05	0.647 ± 0.044	0.774 ± 0.010	0.768 ± 0.020
$\lvert Y_\eta \rvert$	0.73	0.67	0.74 ± 0.10	0.771 ± 0.037	0.633 ± 0.013	0.640 ± 0.024
$\lvert X_{\eta'} \rvert$	0.71	0.61	0.58 ± 0.06	0.436 ± 0.044	0.633 ± 0.013	0.640 ± 0.024
$\lvert Y_{\eta'} \rvert$	0.70	0.79	1.05 ± 0.12	0.900 ± 0.021	0.774 ± 0.010	0.768 ± 0.020

spin structure), and the couplings g and g' for 't Hooft's instanton-induced force with an effective range Λ_{III}. We want to stress that the latter residual interaction only acts on mesons with $J = 0$ as has been stated in [3]. Accordingly we can apply the following scheme for parameter fixing:

1. Choose the quark masses in a physically reasonable range, *i.e.* $m_n \approx 300 \ldots 400\,\mathrm{MeV}$ and $m_s \approx 500 \ldots 600\,\mathrm{MeV}$.
2. Assume an appropriate spin structure that does not conflict with the condition of numerical stability and that provides the correct position of states on the Regge trajectories.
3. Fit the confinement offset and slope to the mesons with $J \neq 0$ and do some fine tuning of the constituent quark masses.
4. Observe the mass spectrum in the scalar and pseudoscalar sector for $g, g' \neq 0$ and fix these coupling constants to the π-K-η-η' mass splittings.

It is crucial for the description of the light meson sector with $J = 0$ that a flavour-dependent force lifts the degeneracies which would otherwise occur in models only assuming confinement and/or one-gluon-exchange potentials. Therefore we include 't Hooft's instanton-induced interaction in the parameter sets of our two model variants, see table 1. They mainly differ in the form assumed for the spin dependence of the confinement force: in model $\mathcal{A}$, a combination of a scalar and a timelike vector structure is adopted as in ref. [6], whereas model $\mathcal{B}$ employs a Fierz invariant and γ_5 invariant spin dependence also investigated by Böhm *et al.* (see [14]) as well as by Gross and Milana (see [15]). A more detailed discussion (especially focussing the radial excitations) will be presented in a separate contribution [16].

In figs. 2 and 3, the effect of the instanton-induced interaction V_{III} is shown for the light pseudoscalar mesons with the parameters of both models. For $g = 0$ and $g' = 0$, the pseudoscalar mesons are bound by confinement only. Therefore the π and the η are degenerate in this limit

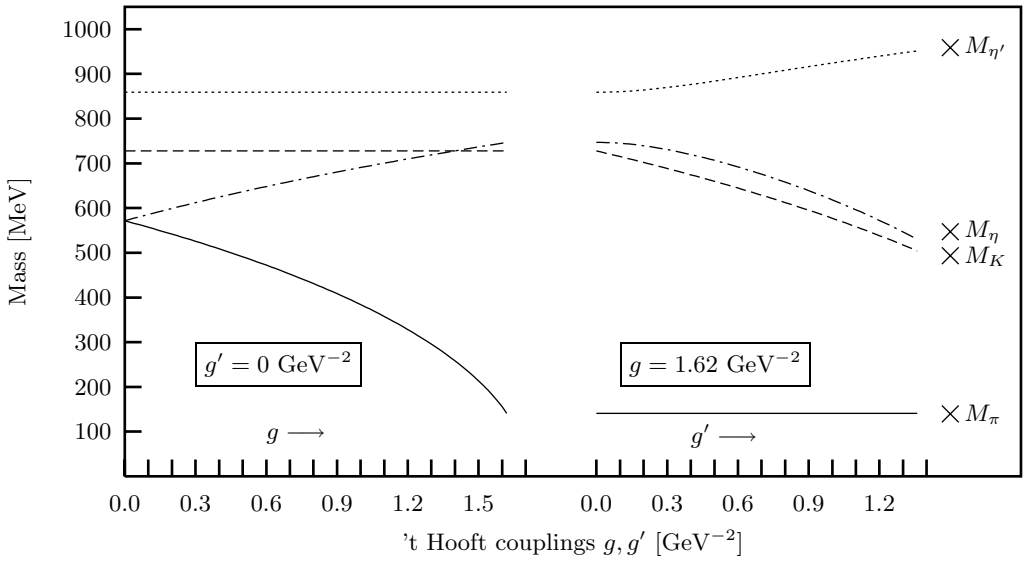

Fig. 3. The effect of 't Hooft's instanton-induced interaction on the masses of the pseudoscalar mesons with the parameters of model $\mathcal{B}$. See also caption of fig. 2.

since no mixing is induced in the isoscalar sector; in a calculation without 't Hooft's interaction, the η is therefore a pure *non-strange* state (*i.e.* $|n\bar{n}\rangle = (|u\bar{u}\rangle + |d\bar{d}\rangle)/\sqrt{2}$). With increasing coupling g, the pion mass is lowered to its experimental value while M_η grows since the underlying effective interaction has an opposite sign for isovector and isoscalar states (see [3] for details). With fixed g, the *non-strange–strange* coupling g' is used to bring simultaneously the masses of the K, η and η' mesons to their experimental values. We stress that a non-vanishing coupling g' not only yields the correct η-η' mass splitting but also induces the expected *non-strange-strange* mixing in the isoscalar sector, see also table 2 for explicit results.

The resulting parameter sets are shown in table 1. Note that the numerical values for the confinement offset and slope, the 't Hooft couplings and the constituent quark masses are comparable for both models although they differ significantly in their confinement spin structure. Let us now briefly discuss the resulting spectra in the isovector, isodublet and isoscalar sectors:

– Both models yield excellent Regge trajectories $M^2 \propto J$, see fig. 4 for the light isovector mesons up to $J = 6$. The complete spectrum with all its radial excitations for light mesons with isospin $I = 1$ is shown in fig. 5 and table 3.
For the $a_0(980)$, we observe a remarkable difference between the models $\mathcal{A}$ and $\mathcal{B}$: in contrast to model $\mathcal{A}$, the spin structure of the parameter set $\mathcal{B}$ obviously allows an interpretation of the a_0 meson as a $q\bar{q}$ state. This is somewhat puzzling since this state is often considered to be a $K\bar{K}$ molecule — an assignment that would be consistent with the fact that we indeed can not describe the $a_0(980)$ with the parameters of model $\mathcal{A}$. We refer to [6] for a detailed discussion of the scalar meson spectrum and its interpretation in the framework of the parameter set $\mathcal{A}$.
– The complete kaonic spectrum is shown in fig. 6 and table 4. We observe a very good agreement with the established experimental data for angular momenta from $J = 0$ to $J = 5$ with one exception: as in the isovector sector, the 0^+ state is lowered significantly in model $\mathcal{B}$ compared to model $\mathcal{A}$. Let us briefly comment on this K_0^* ground state: compared to the PDG value of $M_{K_0^*} \approx 1430\,\text{MeV}$ (see [19]), we find a significant lowering of the mass in model $\mathcal{B}$ compared to model $\mathcal{A}$. Indeed, there is an indication from a recent K-matrix analysis for the scalar nonet that the $IP^\pi = \frac{1}{2}0^+$ ground state actually might be around 1200 MeV (see [20]). Although there are good reasons to compare our results to the "bare poles" of such an analysis where the effects of decay-channel couplings are at least partially taken into account, we have to refrain from a detailed discussion until such an analysis has indeed been performed in all meson sectors.
Furthermore, we note that the calculated states in the K_1 spectrum are each twice degenerate; the present interactions do not distinguish the $S = 0$ and the $S = 1$ states and therefore do not show the experimentally observed splitting. However, we want to mention that an alternative procedure for the regularization of 't Hooft's instanton-induced force seperates these two states; the reason is that the strict $J = 0$ selection rule for this interaction is relaxed if the regularization is applied before evaluating the occuring matrix elements. This effect, although strongly suppressed, yields the correct splittings in the K_1 sector, but we will not discuss further the implications of this slightly modified approach for the residual interaction in our model.

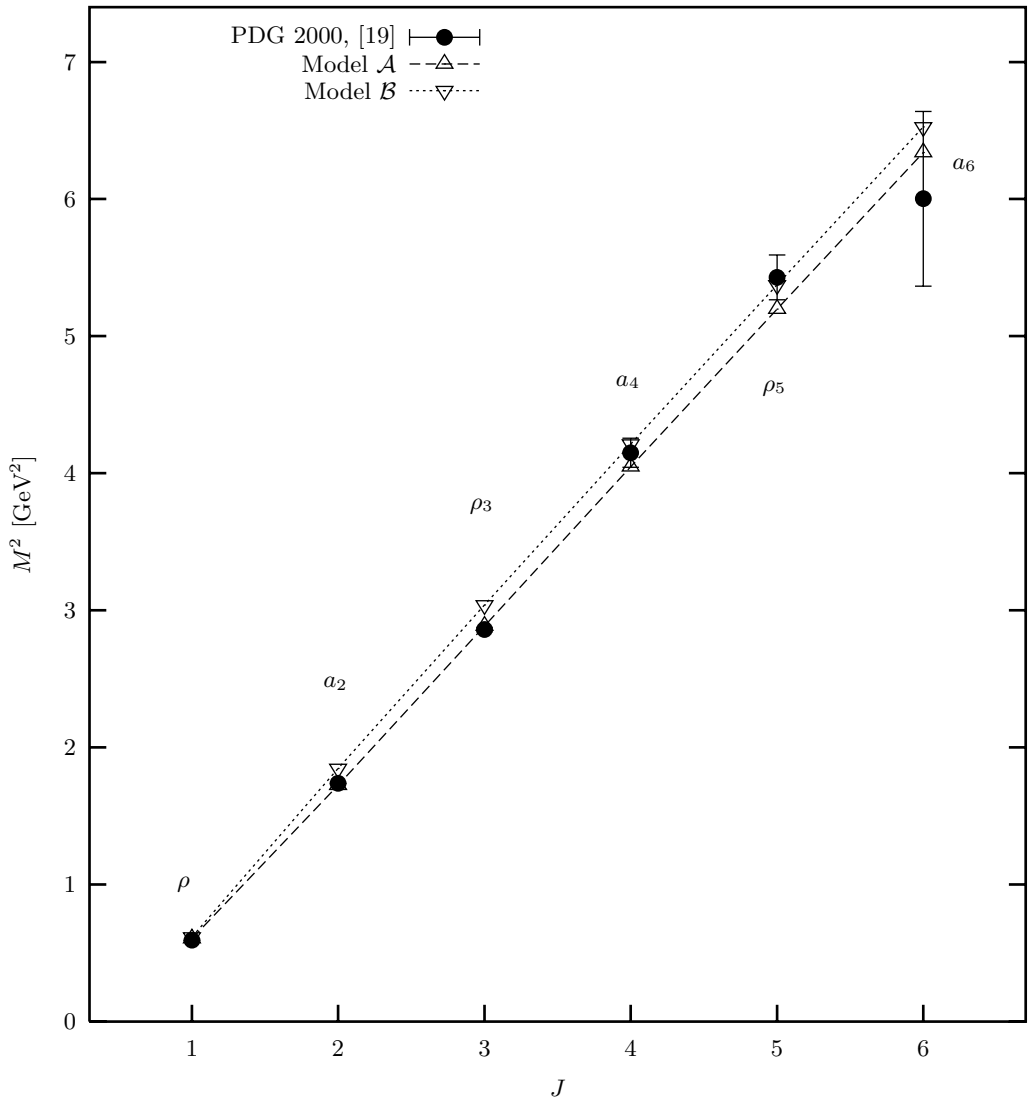

Fig. 4. The Regge trajectory for light isovector mesons with the parameters of model $\mathcal{A}$ and model $\mathcal{B}$ compared to experimental masses from the Particle Data Group (see [19]).

In the PDG listings (see [19]), it is stated that the masses of the K_3 and the K_4 need confirmation; they are therefore omitted in the summary tables. We stress that our calculated masses for these states fit perfectly in a linear Regge plot for the K_J mesons — in contrast to the experimental K_3 and K_4 data shown in fig. 6. We thus support the statement that these have to be considered with caution.

– In fig. 7 and table 5, the results for the isoscalar mass spectra are presented and compared to experimental data. Similar to the pattern in the isovector and isodublet sector, we find a remarkable downward shift of the scalar states in model $\mathcal{B}$ compared to model $\mathcal{A}$. We thus arrive at two alternative interpretations of the scalar isoscalar $q\bar{q}$ spectrum: in model $\mathcal{A}$, we might identify the lowest calculated $IJ^{\pi c} = 00^{++}$ state (mainly flavour singlet) either with the broad structure f_0(400-1200) or with the $f_0(980)$ meson and the second state at ≈ 1500 MeV as a member of the flavour octet; accordingly, this would leave either the $f_0(980)$ or the f_0(400-1200) and the $f_0(1370)$ as non-$q\bar{q}$ state. Let us note that if we furthermore regard the $\gamma\gamma$ decay width and the strong decay width of our lowest f_0 state in model $\mathcal{A}$, we would slightly prefer the $f_0(980)$ to be the $q\bar{q}$ candidate (see [6] and [17]). In model $\mathcal{B}$, we do account for a very low-lying scalar state ("σ meson"), the next excitations to be identified with states around 1250 MeV and 1550 MeV. As mentioned above, model $\mathcal{B}$ also accounts for the $a_0(980)$ meson as a $q\bar{q}$ state whereas this can not be confirmed with the parameters of model $\mathcal{A}$. Clearly, on the basis of the spectrum alone this interpretation can be preliminary at best, especially in view of the complexity in this sector that arises from strong decay channel couplings and possible mixtures with gluonic or other exotic states. A more detailed discussion which also includes numerical results on the strong decay widths of these states will be given in a forthcoming paper (see [17]).

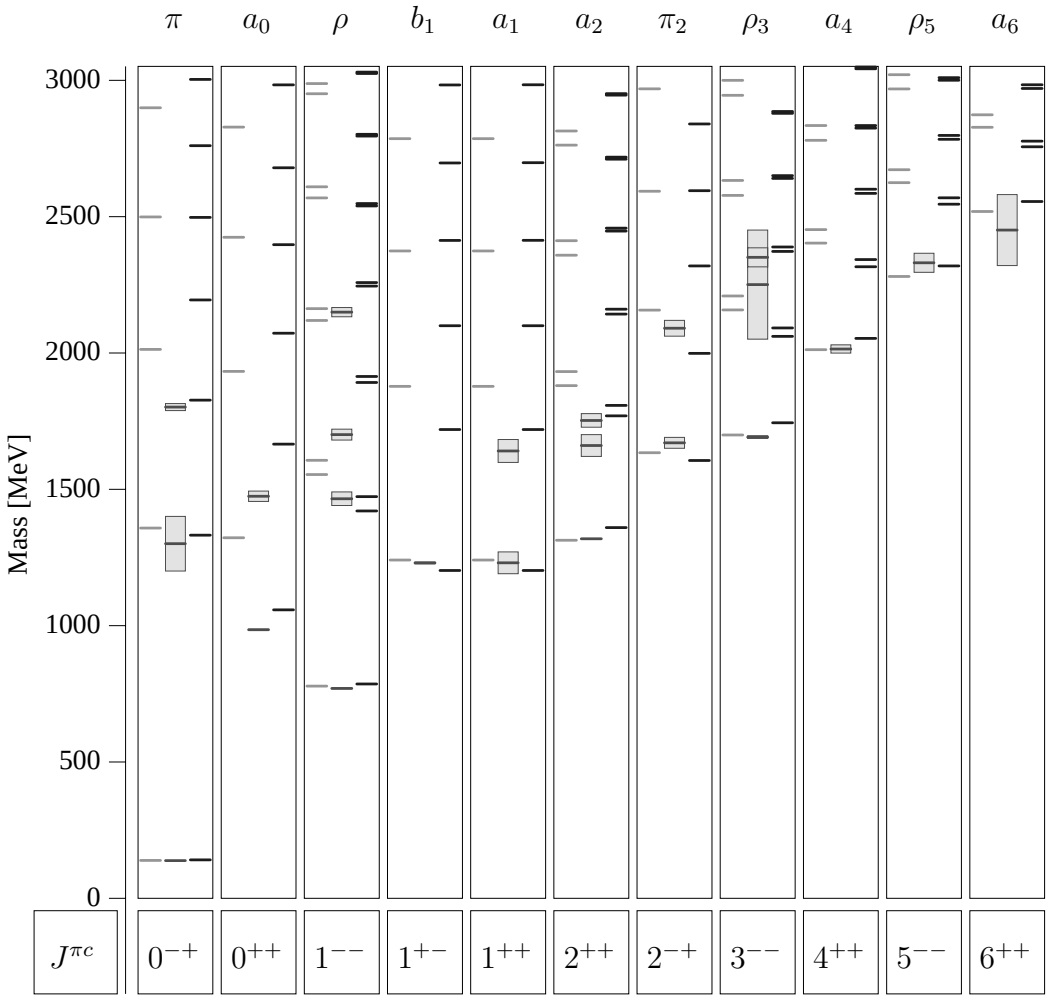

Fig. 5. The spectrum of the light mesons with isospin $I = 1$. Left column for each $J^{\pi c}$: model $\mathcal{A}$; middle column for each $J^{\pi c}$: experimental masses and their error bars marked by the shadowed rectangles from the Particle Data Group (see [19]); right column for each $J^{\pi c}$: model $\mathcal{B}$. Note the difference for the $J^{\pi c} = 0^{++}$ states in the two parameter sets.

Finally we want to comment on the $\eta(1295)$: neither in model $\mathcal{A}$ nor in model $\mathcal{B}$ we can interpret this as a $q\bar{q}$ bound state. Indeed, it has recently been stated in [21] that there is no experimental evidence for an $\eta(1295)$ in the reaction $p\bar{p} \to \pi^+\pi^-\pi^+\pi^-\eta$.

In summary, we find a good overall agreement both in model $\mathcal{A}$ and $\mathcal{B}$. The discrepancies, occuring, *e.g.*, in the K_3 or K_4 masses, can mostly be traced back to questionable $q\bar{q}$ assignments of the considered states. We find the right behaviour with respect to the linear Regge trajectories $M^2 \propto J$ up to highest angular momenta as has been shown in fig. 4. Furthermore, due to the instanton-induced effects our model shows the correct splitting in the pseudoscalar sector independent of the underlying parameter set. The effects of the different Dirac structures of the confinement force in model $\mathcal{A}$ and $\mathcal{B}$ and their implications for the non-relativistic reduction of the Salpeter equation will be discussed in the detailed analysis of ref. [16].

Altogether, a linearly rising confinement potential plus a residual interaction *à la* 't Hooft provides a very satisfacting description of the light $q\bar{q}$ spectra. Therefore we consider our approach based on the Bethe-Salpeter equation in its instantaneous approximation as a trustworthy framework for studying not only meson masses but also their characteristic decays, especially in the pseudoscalar sector.

4 Meson decay properties

In previous publications (see [3,5,10] and [9]), we have studied various mesonic decay properties such as the widths of the decays $\pi^0, \eta, \eta' \to \gamma\gamma$ or the decay constants f_π and f_K. Furthermore, electromagnetic form factors of π and K mesons have been investigated as well as electromagnetic decays like $\rho \to \pi\gamma$ and related processes. We note that instanton-induced vertices in strong decays were also studied (see [8]); a more extensive publication in this context including quark loop contributions is in preparation [17].

Table 3. Masses of the isovector mesons in [MeV], calculated with the parameters of the models $\mathcal{A}$ and $\mathcal{B}$; here, n denotes the radial excitation. For a comparison with the latest experimental data of ref. [19], see fig. 5.

Meson ($J^{\pi c}$)	n	Model $\mathcal{A}$	Model $\mathcal{B}$	Meson ($J^{\pi c}$)	n	Model $\mathcal{A}$	Model $\mathcal{B}$
	0	138	140		0	1240	1201
	1	1357	1331	$b_1(1^{+-})$	1	1876	1718
$\pi(0^{-+})$	2	2012	1826		2	2373	2099
	3	2498	2193				
	4	2898	2496		0	1321	1057
				$a_0(0^{++})$	1	1931	1665
	0	778	785		2	2423	2071
	1	1553	1420				
	2	1605	1472		0	1240	1201
	3	2118	1891	$a_1(1^{++})$	1	1876	1718
$\rho(1^{--})$	4	2161	1913		2	2373	2099
	5	2567	2244				
	6	2608	2257		0	1312	1358
	7	2949	2538	$a_2(2^{++})$	1	1879	1768
	8	2987	2547		2	1931	1807
	0	1633	1605		0	1951	1926
$\pi_2(2^{-+})$	1	2156	1997	$a_3(3^{++})$	1	2401	2247
	2	2592	2318		2	2792	2525
	0	1698	1743		0	2011	2052
	1	2157	2060	$a_4(4^{++})$	1	2402	2315
$\rho_3(3^{--})$	2	2208	2091		2	2451	2341
	3	2576	2371				
	4	2631	2388		0	2463	2444
				$a_5(5^{++})$	1	2825	2685
	0	2279	2318		2	3153	2905
	1	2623	2545				
$\rho_5(5^{--})$	2	2671	2568		0	2517	2554
	3	2967	2782	$a_6(6^{++})$	1	2826	2755
	4	3019	2797		2	2872	2776

We want to extend these approaches to other processes where $q\bar{q}$ bound states are involved. Firstly, we will pick up the recent discussion of the pseudoscalar decay constants (see [22] and [23]) and quote our results for the η and the η' meson for their *non-strange* and *strange* content separately. We will review the two-photon decay of $J^\pi = 0^-$ mesons and the related transition form factors at various photon virtualities in sect. 4.2 where our results for $-q_i^2 \to \infty$ will be linked to the pseudoscalar decay constants. We present the electromagnetic form factors of the charged π and K mesons for the sake of completeness since they have not been published yet in the parameter sets that we adopt in this paper. For the same reason, we also present new results on the electromagnetic decay widths of the processes $\mathcal{M} \to \mathcal{M}'\gamma$ that have already been studied in ref. [5]. Then, we will comment on the weak decays $\pi^+/K^+ \to e^+\nu_e\gamma$ before we finally investigate our results on the form factors of the so-called $K_{\ell 3}$ decay.

Let us stress that these calculations concerning meson decay properties are done in the parameter sets $\mathcal{A}$ and $\mathcal{B}$ that were completely fixed with regard to the experimental meson mass spectra. We do therefore not introduce new parameters or alter the models discussed in the previous section since we aim at a global description of meson masses as well as their characteristic decays.

4.1 Pseudoscalar decay constants

In recent years, the question of pseudoscalar decay constants — especially those of the η and η' mesons — was discussed in numerous publications (see, *e.g.*, [22,23], and references therein). It has become clear that due to the mixing in the isoscalar sector, the contributions of the *non-strange* and the *strange* content (or the singlet and octet contributions in an alternate mixing scheme) have to be distinguished.

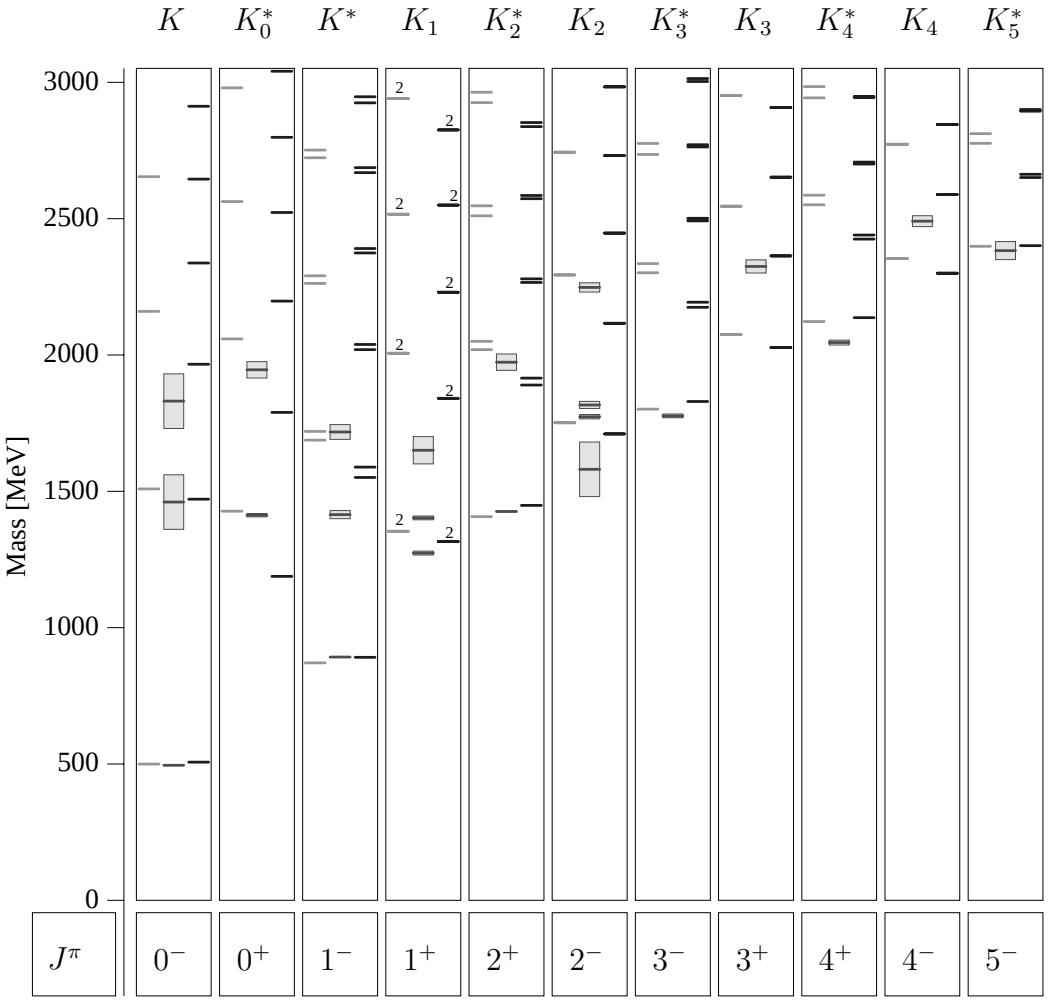

Fig. 6. The spectrum of the light mesons with isospin $I = \frac{1}{2}$. Left column for each J^π: model $\mathcal{A}$; middle column for each J^π: experimental masses and their error bars marked by the shadowed rectangles from the Particle Data Group (see [19]); right column for each J^π: model $\mathcal{B}$. The experimental data for the K_3 and K_4 masses need confirmation; the PDG data plotted above do not fit in a linear Regge trajectory $M^2_{K_J} \propto J$. Note that the calculated K_1 states are each 2-fold degenerate for spin $S = 0$ and $S = 1$, indicated by "2", so that the total number of K_1 states is correct; see the discussion in sect. 3.

Let us start our discussion with the definition of the pseudoscalar decay constant with the axial current $A^\pi_\mu = \bar{u}\gamma_\mu\gamma_5 d$ for a pion with positive charge:

$$\langle 0|A^\pi_\mu|\pi^+(p)\rangle = ip_\mu f_\pi \,. \tag{14}$$

In a similar way, one can define the decay constant of the $K^\pm$ meson; these constants are related with the corresponding decay constants for the neutral mesons via $f_{\mathcal{M}^0} = f_{\mathcal{M}^\pm}/\sqrt{2}$ for $\mathcal{M} = \pi, K$.

Due to the instantaneous approximation, f_π can be derived from the pion's Salpeter amplitude $\Phi_{(\pi)}(\vec{p})$ in the rest frame of the meson:

$$f_\pi = \frac{\sqrt{3}}{M_\pi}\int\frac{\mathrm{d}^4p}{(2\pi)^4}\mathrm{tr}\left[S_1^F\left(\frac{P}{2}+p\right)\Gamma^P_{(\pi)}(p)S_2^F\left(-\frac{P}{2}+p\right)\gamma_0\gamma_5\right]$$
$$\stackrel{P=(M,\vec{0})}{=} \frac{\sqrt{3}}{M_\pi}\int\frac{\mathrm{d}^3p}{(2\pi)^3}\mathrm{tr}\left[\Phi_{(\pi)}(\vec{p})\gamma_0\gamma_5\right] \,, \tag{15}$$

where the trace is evaluated only on Dirac indices. It can be shown analytically that the latter expression is proportional to the difference of the upper and lower component of the equal-time wave function of the pion (see [2]). Therefore, f_π is highly sensitive to relativistic ingredients of the model in which it is calculated; in non-relativistic models, the evaluation fails typically by orders of magnitude. As has been shown in refs. [2] and [3], the electromagnetic decay widths for $\rho, \omega, \phi \to e^+e^-$ can be treated in a similar way; the numerical results for the parameter sets $\mathcal{A}$ and $\mathcal{B}$ of this work are comparable to the widths of model V2 in these previous publications.

In table 6, the results for f_π and f_K are shown for the parameters of model $\mathcal{A}$ and $\mathcal{B}$; obviously, we overestimate these observables by a factor of ≈ 1.5 which is typical for models with large constituent quark masses as found here, see [3]. Although our relativistic ansatz improves dramatically the result compared to non-relativistic calculations,

Table 4. Masses of the isodublet mesons in [MeV], calculated with the parameters of the models $\mathcal{A}$ and $\mathcal{B}$; here, n denotes the radial excitation. For a comparison with the latest experimental data of ref. [19], see fig. 6. Note that the calculated K_1 states are each 2-fold degenerate for spin $S = 0$ and $S = 1$.

Meson (J^π)	n	Model $\mathcal{A}$	Model $\mathcal{B}$	Meson (J^π)	n	Model $\mathcal{A}$	Model $\mathcal{B}$
	0	499	506		0	1426	1187
	1	1508	1470	$K_0^*(0^+)$	1	2058	1788
	2	2159	1965		2	2561	2196
$K(0^-)$	3	2652	2336				
	4	3062	2644		0	870	890
	5	3420	2911		1	1687	1550
	6	3748	3151	$K^*(1^-)$	2	1718	1588
	7	4074	3370		3	2261	2018
					4	2289	2037
	0	1353	1315				
	1	1353	1315		0	1406	1447
$K_1(1^+)$	2	2005	1840	$K_2^*(2^+)$	1	2019	1889
	3	2005	1840		2	2049	1914
	0	1750	1709		0	1800	1828
$K_2(2^-)$	1	1750	1709	$K_3^*(3^-)$	1	2300	2173
	2	2292	2115		2	2334	2192
	0	2074	2026		0	2121	2136
$K_3(3^+)$	1	2074	2026	$K_4^*(4^+)$	1	2550	2424
	2	2544	2362		2	2585	2439
	0	2352	2299		0	2397	2400
$K_4(4^-)$	1	2352	2299	$K_5^*(5^-)$	1	2775	2649
	2	2771	2587		2	2811	2661

we find in these results a shortcoming of our model which might be related to the instantaneous approximation of the underlying Bethe-Salpeter equation and/or our refraining from "running quark masses".

Now let us focus the η and the η' meson, respectively. As we have already emphasized, mixing between the *non-strange* and the *strange* sector is crucial for the understanding of the isoscalar states. We adopt the flavour decomposition

$$|\eta\rangle = X_\eta|n\rangle + Y_\eta|s\rangle\,, \qquad |\eta'\rangle = X_{\eta'}|n\rangle + Y_{\eta'}|s\rangle\,, \quad (16)$$

where $|n\rangle := (|u\bar{u}\rangle + |d\bar{d}\rangle)/\sqrt{2}$ and $|s\rangle := |s\bar{s}\rangle$; the coefficients obey $X_{\mathcal{M}}^2 + Y_{\mathcal{M}}^2 = 1$ ($\mathcal{M} = \eta, \eta'$). In table 2, we compare the coefficients, extracted from our calculated Salpeter amplitudes, with experimental numbers from the Mark III (see [25]) and the DM2 (see [26]) collaborations. The coefficients X_η and Y_η in model $\mathcal{A}$ and model $\mathcal{B}$ are consistent with the findings of the experimental analysis whereas the η' mixing seems to be described not that well in model $\mathcal{A}$. Note that there are also some new estimates for these coefficients based on a phenomenological analysis of the availiable world data. They are also quoted in table 2 and show that the experimental determination might be not unique in a strict sense. However, it should be added that these new results are found in the so-called one-angle mixing scheme with

$$\begin{pmatrix} |\eta\rangle \\ |\eta'\rangle \end{pmatrix} = \begin{pmatrix} \cos\phi & -\sin\phi \\ \sin\phi & \cos\phi \end{pmatrix} \begin{pmatrix} |n\rangle \\ |s\rangle \end{pmatrix}\,, \quad (17)$$

where by definition $|X_\eta| = |Y_{\eta'}|$ and $|Y_\eta| = |X_{\eta'}|$ hold so that the numerical values of ref. [22] and [24] have to be considered with care. Indeed we find that η and η' are not simply related by a flavour rotation; in our calculation, the radial amplitudes of these isoscalar states differ considerably.

Therefore, adopting the general mixing scheme of eq. (16), we define the decay constants for the η and the η' meson as follows:

$$\langle 0|A_\mu^j|\mathcal{M}(p)\rangle = ip_\mu f_{\mathcal{M}}^j \quad (\, j = n, s\,; \quad \mathcal{M} = \eta, \eta'\,)\,, \quad (18)$$

with $A_\mu^n = (\bar{u}\gamma_\mu\gamma_5 u + \bar{d}\gamma_\mu\gamma_5 d)/\sqrt{2}$ and $A_\mu^s = \bar{s}\gamma_\mu\gamma_5 s$. In practice, these constants are computed as in eq. (15). In table 6, we present our results using the parameters of the models $\mathcal{A}$ and $\mathcal{B}$. We stress that the quoted results of [22] are found in the one-angle mixing scheme of eq. (17) so

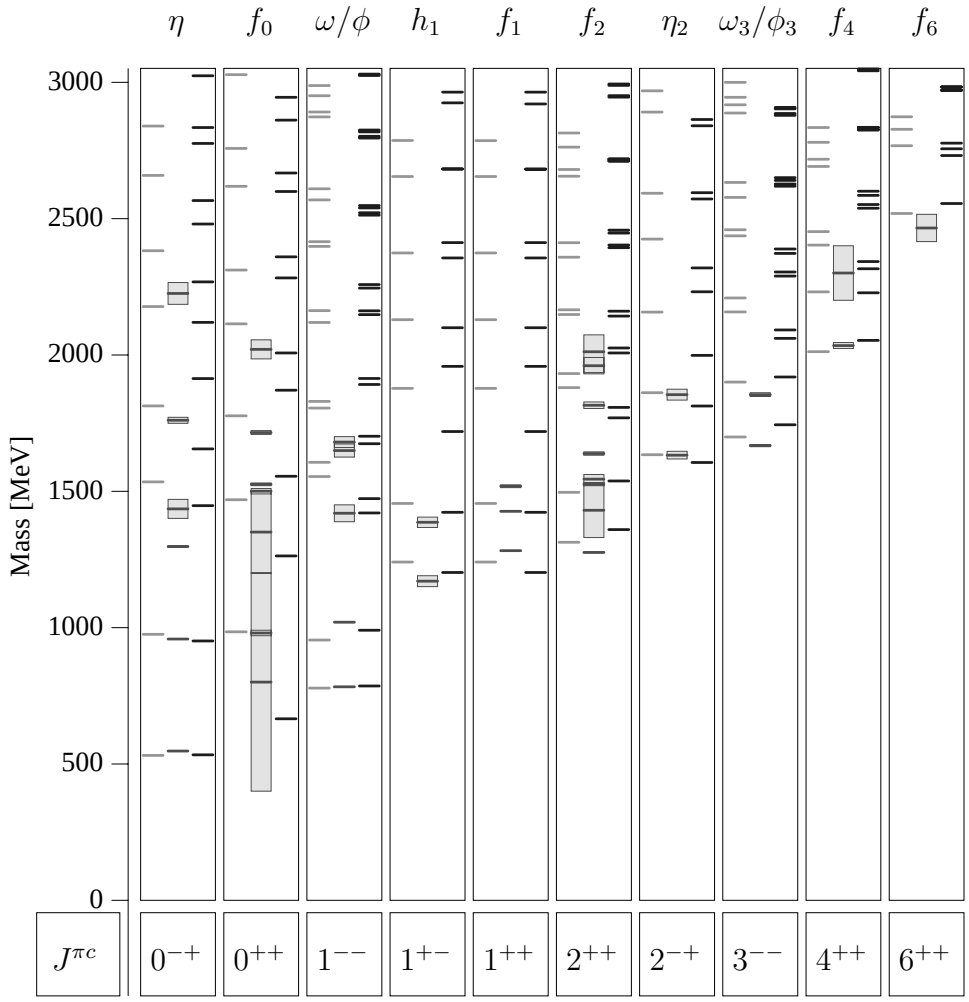

Fig. 7. The spectrum of the light mesons with isospin $I = 0$. Left column for each $J^{\pi c}$: model $\mathcal{A}$; middle column for each $J^{\pi c}$: experimental masses and their error bars marked by the shadowed rectangles from the Particle Data Group (see [19]); right column for each $J^{\pi c}$: model $\mathcal{B}$. There are experimental hints that the $\eta(1295)$ (plotted above according to the PDG data) might not really exist, see [21].

that a comparison with our ansatz has to be done with some caution. We conclude that although f_π and f_K are overestimated in our model, we find plausible results of roughly the same quality for the η and η' decay constants compared to [22] due to the instanton-induced mixing of these isoscalar states.

4.2 Two-photon decays

In this section, we will discuss the two photon decays of pseudoscalar mesons not only for two real photons in the final state ($q_1^2 = q_2^2 = 0$) but also the 0^- transition form factors in the case that either one ($q_1^2 = 0$, $q_2^2 \neq 0$) or both ($q_1^2 \neq 0$, $q_2^2 \neq 0$) of the photons are virtual.

In fig. 8, the $\gamma\gamma$ decay of pseudoscalar mesons is shown, calculated in lowest order in the Mandelstam formalism (see [18]). The related matrix element for the transition $\mathcal{M} \to \gamma\gamma$ with $\mathcal{M} = \pi^0, \eta, \eta'$ reads

$$T^{\mathcal{M}}_{\gamma\gamma}(q_1, q_2) = i\sqrt{3} \int \frac{\mathrm{d}^4 p}{(2\pi)^4} \times \mathrm{tr}\Big[S^F\Big(\frac{P}{2}+p\Big) \Gamma^P_{(\mathcal{M})}(p) S^F\Big(-\frac{P}{2}+p\Big) \not{\varepsilon}_2 S^F\Big(\frac{P}{2}+p-q_1\Big) \not{\varepsilon}_1 + S^F\Big(\frac{P}{2}+p\Big) \Gamma^P_{(\mathcal{M})}(p) S^F\Big(-\frac{P}{2}+p\Big) \not{\varepsilon}_1 S^F\Big(\frac{P}{2}+p-q_2\Big) \not{\varepsilon}_2 \Big], \tag{19}$$

where $\Gamma^P_{(\mathcal{M})}(p)$ is the vertex function for the pseudoscalar meson $\mathcal{M}$ defined in eq. (12). The polarization vectors ε_i obey $\varepsilon_i^2 = -1$ and $\varepsilon_i \cdot k_i = 0$ $(i = 1, 2)$ for real photons. Here, the factor $\sqrt{3}$ originates from the trace over colour indices; the trace in eq. (19) is understood with respect to Dirac and flavour indices.

From Lorentz invariance, it is possible to derive another expression for this matrix element for pseudoscalar

Table 5. Masses of the isoscalar mesons in [MeV], calculated with the parameters of the models $\mathcal{A}$ and $\mathcal{B}$; here, n denotes the radial excitation. For a comparison with the latest experimental data of ref. [19], see fig. 7.

Meson ($J^{\pi c}$)	n	Model $\mathcal{A}$	Model $\mathcal{B}$	Meson ($J^{\pi c}$)	n	Model $\mathcal{A}$	Model $\mathcal{B}$
	0	531	533		0	984	665
	1	975	950		1	1468	1262
	2	1533	1446		2	1776	1554
	3	1812	1654	$f_0(0^{++})$	3	2113	1870
$\eta(0^{-+})$	4	2177	1912		4	2310	2006
	5	2381	2118		5	2617	2281
	6	2657	2267		6	2756	2359
	7	2838	2479				
	8	3054	2565		0	1240	1201
				$f_1(1^{++})$	1	1454	1422
	0	778	785		2	1876	1718
	1	954	990				
	2	1553	1420		0	1312	1358
	3	1605	1472		1	1495	1537
$\omega/\phi(1^{--})$	4	1804	1674		2	1879	1768
	5	1829	1701		3	1931	1807
	6	2118	1891		4	2147	2006
	7	2161	1913		5	2164	2025
				$f_2(2^{++})$	6	2357	2141
	0	1633	1605		7	2411	2160
$\eta_2(2^{-+})$	1	1861	1812		8	2654	2392
	2	2156	1997		9	2679	2402
					10	2761	2446
	0	1698	1743		11	2813	2457
	1	1899	1918				
$\omega_3/\phi_3(3^{--})$	2	2157	2060		0	1951	1926
	3	2208	2091	$f_3(3^{++})$	1	2192	2127
					2	2401	2247
	0	2223	2200				
	1	2478	2398		0	2011	2052
$\eta_4(4^{-+})$	2	2622	2475		1	2230	2227
	3	2917	2700	$f_4(4^{++})$	2	2402	2315
					3	2451	2341
	0	2279	2318				
	1	2514	2493		0	2463	2444
$\omega_5/\phi_5(5^{--})$	2	2623	2545	$f_5(5^{++})$	1	2730	2640
	3	2671	2568		2	2825	2685
	0	1240	1201		0	2517	2554
$h_1(1^{+-})$	1	1454	1422	$f_6(6^{++})$	1	2766	2730
	2	1876	1718		2	2826	2755

mesons

$$T^{\mathcal{M}}_{\gamma\gamma}(q_1,q_2) = \alpha\epsilon_{\mu\nu\alpha\beta}\varepsilon_1^{\mu}(q_1)\varepsilon_2^{\nu}(q_2)q_1^{\alpha}q_2^{\beta}\cdot F^{\mathcal{M}}_{\gamma\gamma}(q_1^2,q_2^2)\,, \quad (20)$$

in terms of the transition form factor $F^{\mathcal{M}}_{\gamma\gamma}(q_1^2,q_2^2)$; here, α is the fine-structure constant. With this last equation, it is now possible to relate our matrix element calculated via eq. (19) with the transition form factor and the decay width defined by

$$\Gamma^{\mathcal{M}}_{\gamma\gamma}(Q_1^2,Q_2^2) = \alpha^2\frac{M^3_{\mathcal{M}}}{64\pi}\left|F^{\mathcal{M}}_{\gamma\gamma}(Q_1^2,Q_2^2)\right|^2\,, \text{ with } Q_i^2 := -q_i^2. \quad (21)$$

It is worth noting that in a similar way it is possible to calculate the two photon widths $\Gamma_{\gamma\gamma}$ in our relativistic quark model not only for $J^{\pi} = 0^-$ mesons but also for $J^{\pi} = 0^+, 2^{\pm}, 4^{\pm}\ldots$ mesons (including $c\bar{c}$ and $b\bar{b}$ bound states with an additional one-gluon-exchange potential) and their radial excitations in reasonable agreement with the (rare) experimental data (see [9]).

In table 7, we show our results for the widths of the decays $\pi^0, \eta, \eta' \to \gamma\gamma$ into two real photons; obviously, we underestimate these widths and as for the pseudoscalar decay constants, we find a discrepancy of about a factor of 1.5 in the amplitude. Indeed, this can be understood

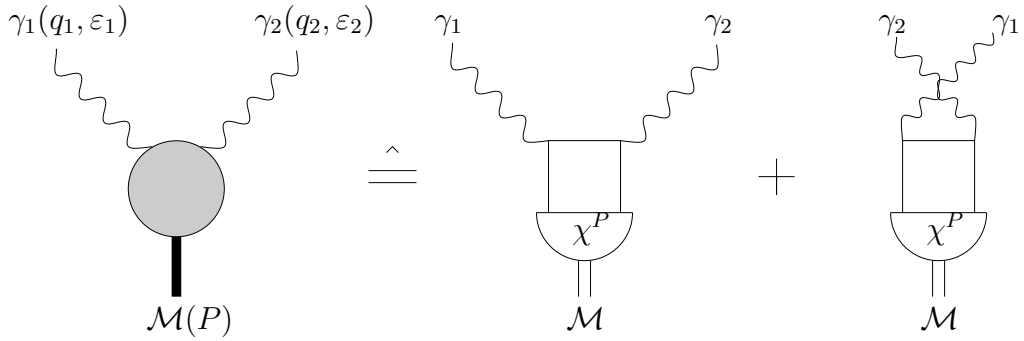

Fig. 8. The decay $\mathcal{M}(P) \to \gamma_1(q_1,\varepsilon_1)\gamma_2(q_2,\varepsilon_2)$ in lowest order in the Mandelstam formalism.

with the results of the foregoing subsection since — *e.g.* for the pion — the relation $\Gamma^{\pi^0}_{\gamma\gamma}(0,0) \propto 1/f_\pi^2$ holds. From fig. 9, one observes that for all Q^2 the two photon width $\Gamma^{\pi^0}_{\gamma\gamma}(Q^2) := \Gamma^{\pi^0}_{\gamma\gamma}(Q^2 := Q_1^2, 0)$ is underestimated. We conclude that for a deeply bound particle such as the pion the instantaneous approximation shows up its shortcomings although the meson Salpeter amplitudes are correctly boosted. We also present the widths for the scalar meson decays $f_0(400\text{-}1200), f_0(980), a_0(980) \to \gamma\gamma$ in table 7. Note that each of these decays can only be calculated in one of the parameter sets $\mathcal{A}$ or $\mathcal{B}$ due to the different $q\bar{q}$ assignments to the mesons in the scalar sector in both models, see sect. 3.

Let us now study these results in some more detail. In ref. [27], Brodsky and Lepage presented the well-known and parameter-free interpolation formula for the pion transition form factor:

$$F^{\pi^0}_{\gamma\gamma}(Q^2,0) = \frac{6C_\pi f_\pi}{Q^2 + 4\pi^2 f_\pi^2}\,, \tag{22}$$

with the charge factor $C_\pi := 1/(3\sqrt{2})$ coming from the quark flavours. Although Brodsky *et al.* recently proposed a slightly modified version of this formula (see [28]), it works quite well in its original version and leads to the famous limit

$$\lim_{Q^2\to\infty} Q^2 F^{\pi^0}_{\gamma\gamma}(Q^2,0) = 6C_\pi f_\pi = 2f_{\pi^0} \tag{23}$$

for the form factor of the decay $\pi^0 \to \gamma\gamma^*$ in the asymptotic region; note that here $f_{\pi^0} := f_\pi/\sqrt{2} \approx 93\,\text{MeV}$. On the other hand, we recover $\Gamma^{\pi^0}_{\gamma\gamma}(Q^2 \to 0, 0) \propto 1/f_\pi^2$ with eqs. (21) and (22) for real photons as quoted above.

For the η and the η', the situation is somewhat different. Since these isoscalar mesons are mixed *non-strange/strange* states, one has to distinguish between the contributions of different flavour structures, see eq. (16). In [29], the authors propose a two-pole interpolation formula for the η/η' transition form factors yielding

$$\lim_{Q^2\to\infty} Q^2 F^{\mathcal{M}}_{\gamma\gamma}(Q^2,0) = 6C_n f^n_{\mathcal{M}} + 6C_s f^s_{\mathcal{M}} \tag{24}$$

for $\mathcal{M} = \eta, \eta'$ in the asymptotic limit. Here, $f^j_{\mathcal{M}}$, with $j = n, s$ are the decay constants defined in eq. (18) and

Table 6. The pseudoscalar decay constants of the π, K, η and η' mesons, calculated with the parameters of the models $\mathcal{A}$ and $\mathcal{B}$. The results of ref. [22] originate from a phenomenological analysis of various decay ratios, *e.g.*, $\Gamma(J/\psi \to \eta'\rho)/\Gamma(J/\psi \to \eta\rho)$; note that these numerical values are found in the so-called one-angle mixing scheme, see eq. (17).

Decay constant	Model $\mathcal{A}$	Model $\mathcal{B}$	PDG 2000 [19]	Ref. [22]
f_π [MeV]	212	219	130.7 ± 0.46	—
f_K [MeV]	248	238	159.8 ± 1.88	—
f^n_η [MeV]	142	161	—	108.5 ± 2.6
f^s_η [MeV]	−205	−166	—	−111.2 ± 5.5
$f^n_{\eta'}$ [MeV]	92	95	—	88.8 ± 2.5
$f^s_{\eta'}$ [MeV]	166	176	—	136.8 ± 6.4

$C_n = 5/(9\sqrt{2})$ and $C_s = 1/9$ are charge factors coming from the *non-strange/strange* quark flavours. If we compare our numerical results for the left-hand side of eq. (24) and for the right-hand side from the values of table 6, we find that we do not obtain the right limit as $Q^2 \to \infty$ for the transition form factors (*e.g.*, $Q^2 F^{\pi^0}_{\gamma\gamma}(Q^2 \to \infty, 0) \approx 70\,\text{MeV}$ but $6C_\pi f_\pi \approx 150\,\text{MeV}$ in both models). We want to stress that, nevertheless, we find a good agreement with the experimental results for $Q^2 F^{\mathcal{M}}_{\gamma\gamma}(Q^2)$ or $\Gamma^{\mathcal{M}}_{\gamma\gamma}(Q^2)$, respectively, for $\mathcal{M} = \eta, \eta'$ — see fig. 9.

Finally, we want to comment on the decay of a $J^\pi = 0^-$ meson into two virtual photons. We will focus on the case of identical virtuality of the outgoing photons ($Q_1^2 = Q_2^2 =: Q^2$) but we want to emphasize that in general the whole Q_1^2-Q_2^2 plane can be calculated in our model. A result for $Q^2 \to \infty$ from operator product expansion yields

$$\lim_{Q^2\to\infty} Q^2 F^{\pi^0}_{\gamma\gamma}(Q^2,Q^2) = 2C_\pi f_\pi \tag{25}$$

for the transition form factor of the pion (see [34] and [35]). We can confirm this result in our calculations in contrast to the limits of the foregoing discussion since now

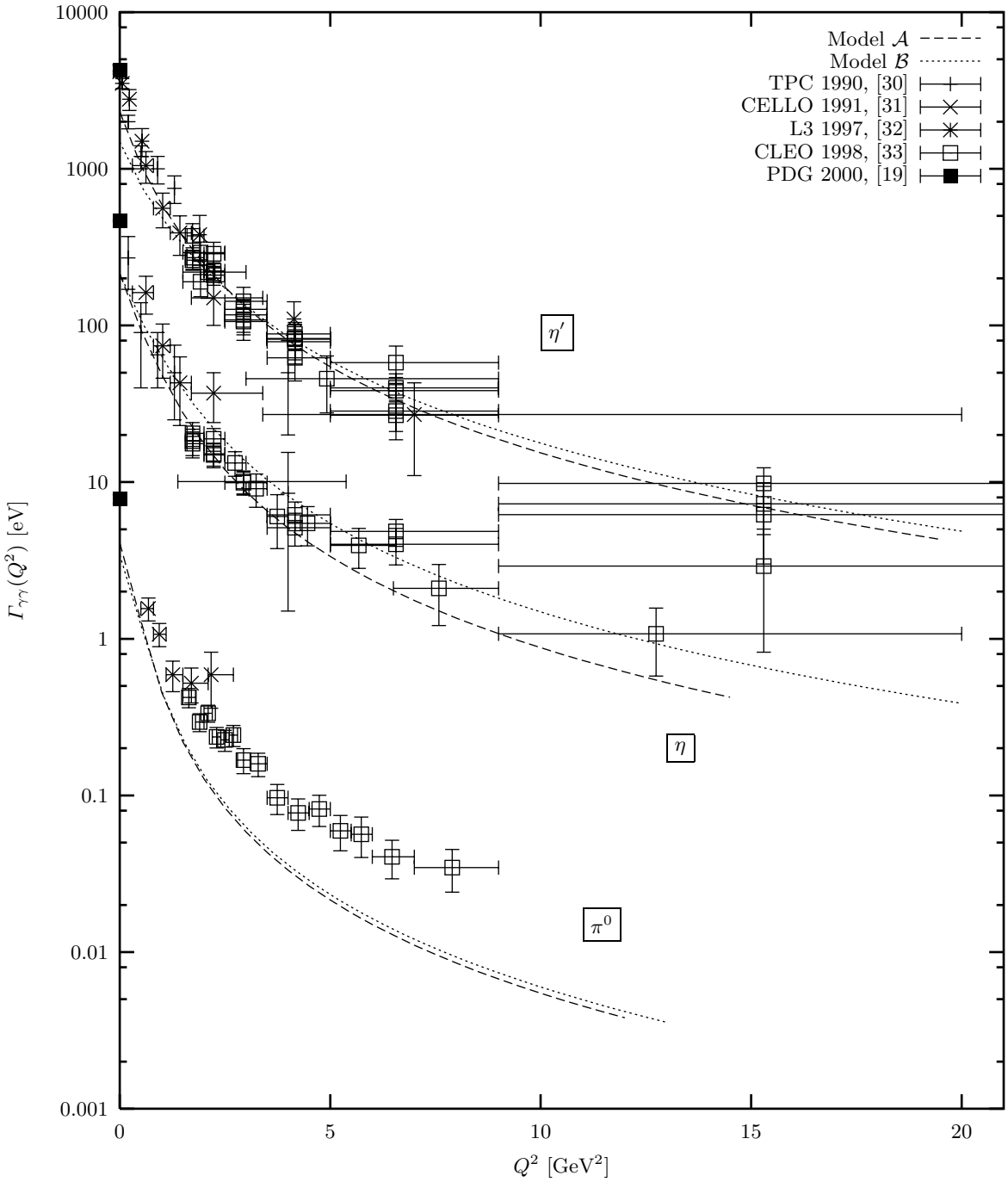

Fig. 9. The decay widths for the processes $\pi^0, \eta, \eta' \to \gamma\gamma^*$ as a function of the momentum transfer of the virtual photon, calculated with the parameters of model $\mathcal{A}$ and model $\mathcal{B}$.

the virtuality distribution of the two outgoing photons is symmetric even at very large Q^2. Furthermore, we can give a similar relation for the form factor of the decays $\eta, \eta' \to \gamma^*\gamma^*$ in the limit of large Q^2 from analytical considerations in the framework of our model (see the Appendix for details):

$$\lim_{Q^2\to\infty} Q^2 F_{\gamma\gamma}^{\mathcal{M}}(Q^2, Q^2) = 2C_n f_{\mathcal{M}}^n + 2C_s f_{\mathcal{M}}^s \,, \qquad (26)$$

for $\mathcal{M} = \eta, \eta'$; the charge factors C_j and the decay constants $f_{\mathcal{M}}^j$ $(j = n, s)$ are defined as above. In figs. 10 and 11, these form factors are plotted together with their limits for large Q^2 with model $\mathcal{A}$ and $\mathcal{B}$; no experimental data exist in this kinematical region so far. Obviously, the numerically evaluated form factors in both models indeed show up the limits that we found in our analytical calculations, see the Appendix.

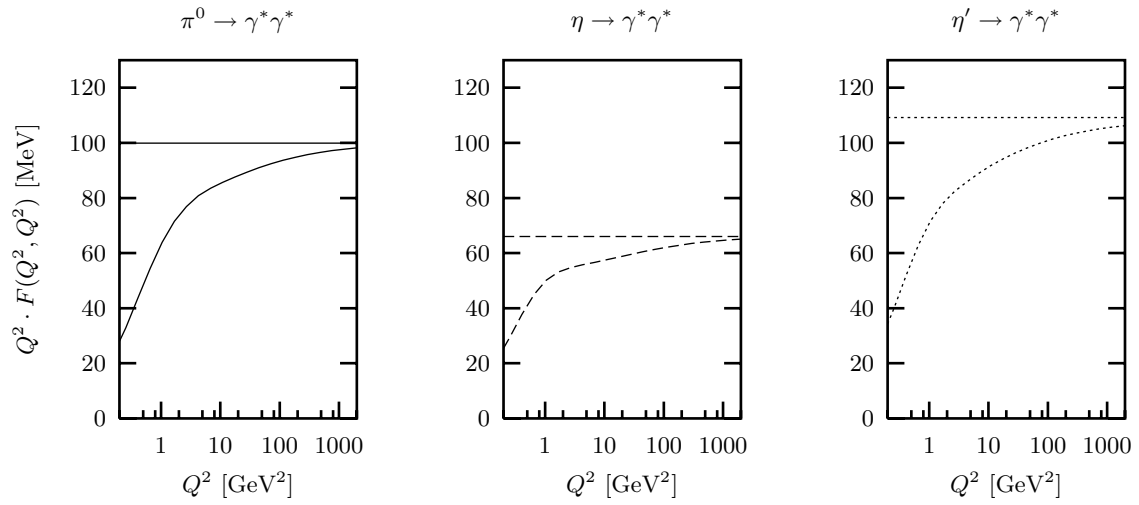

Fig. 10. The form factors of the $\gamma^*\gamma^*$ decays at equal photon virtualities $Q^2 := Q_1^2 = Q_2^2$, calculated with model $\mathcal{A}$, and their limits for $Q^2 \to \infty$ according to the eqs. (25) and (26), denoted by the horizontal lines.

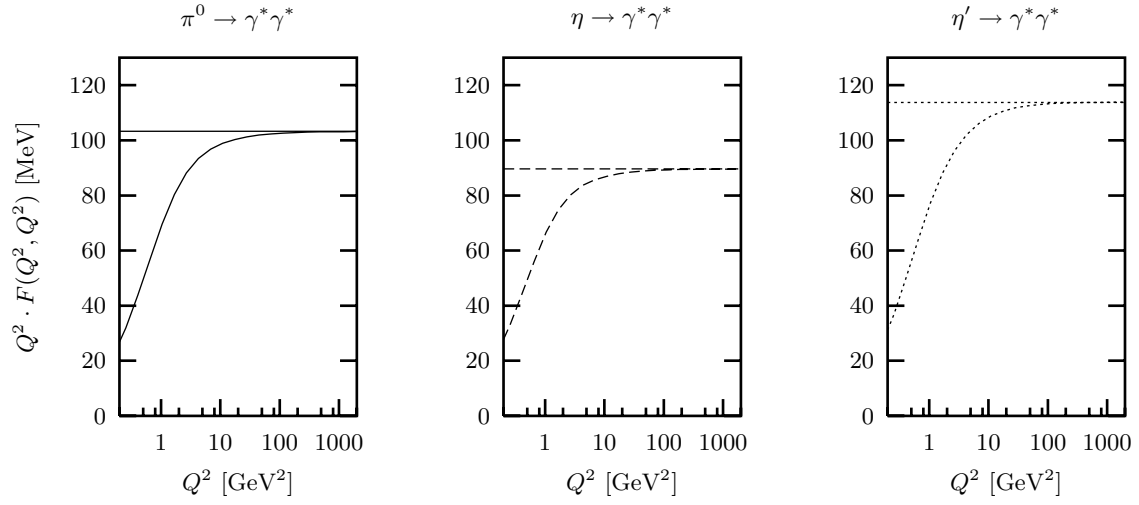

Fig. 11. The form factors of the $\gamma^*\gamma^*$ decays at equal photon virtualities $Q^2 := Q_1^2 = Q_2^2$, calculated with model $\mathcal{B}$, and their limits for $Q^2 \to \infty$ according to the eqs. (25) and (26), denoted by the horizontal lines.

4.3 The electromagnetic form factors of the charged π and K mesons

For the sake of completeness, we want to present the electromagnetic form factors of the $\pi^\pm$ and the $K^\pm$ in this section since they have not been published in the models $\mathcal{A}$ and $\mathcal{B}$ up to now.

The meson form factors for the transitions $\pi^\pm(P) \to \pi^\pm(P')\gamma^*(q)$ and $K^\pm(P) \to K^\pm(P')\gamma^*(q)$ with a (spacelike) photon virtuality $q^2 = (P - P')^2 =: -Q^2 < 0$ are defined as follows:

$$\langle \mathcal{M}(P') \left| J_\mu(0) \right| \mathcal{M}(P) \rangle = \mathcal{Q} F_{\mathcal{M}}(Q^2) \left(P + P'\right)_\mu \,. \quad (27)$$

Here, $P(P')$ is the four-momentum of the incoming (outgoing) meson $\mathcal{M} = \pi^\pm, K^\pm$; the factor $\mathcal{Q} = e_1 + e_2$ denotes the meson charge. As has been shown in ref. [5], we derive this matrix element in the Bethe-Salpeter approach via the Mandelstam formalism (see [18]) on the basis of a

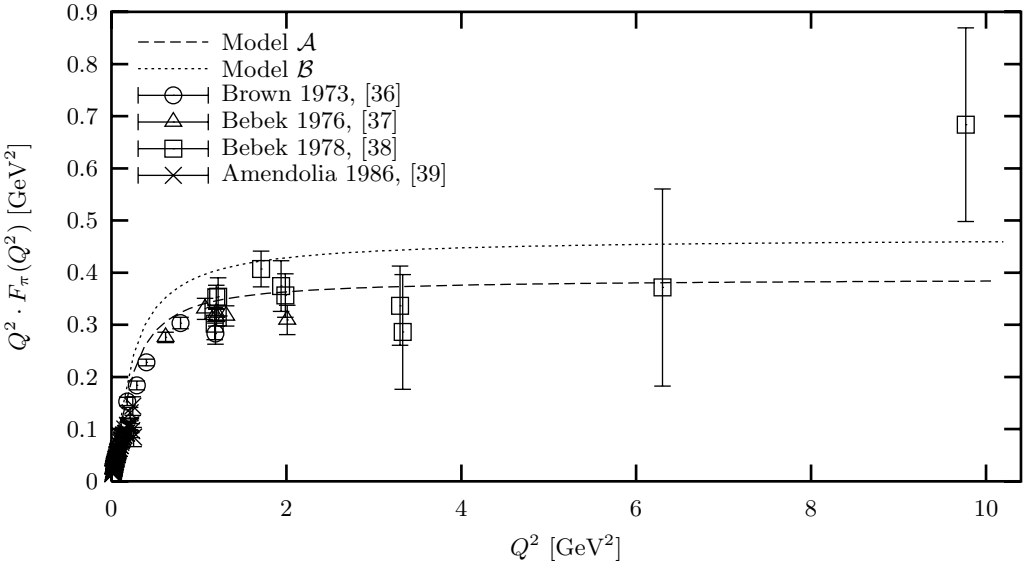

Fig. 12. The electromagnetic form factor $Q^2 \cdot F_\pi(Q^2)$ of the charged pion, calculated with the parameters of model $\mathcal{A}$ and model $\mathcal{B}$. Note that the correct shape of the form factor beyond $\approx 1\,\mathrm{GeV}^2$ can be traced back to the application of the full Lorentz boost, see [5].

Table 7. The widths of the decays $0^\pi \to \gamma\gamma$ ($\pi = \pm$), calculated with the parameters of the models $\mathcal{A}$ and $\mathcal{B}$. Experimental widths marked with (*) are quoted in ref. [19] without using them for averages, fits etc. The interpretation of the scalar mesons differ in models $\mathcal{A}$ and $\mathcal{B}$ such that not all widths are calculated in both parameter sets.

Decay width	Model $\mathcal{A}$	Model $\mathcal{B}$	PDG 2000 [19]
$\Gamma(\pi \to \gamma\gamma)$ [eV]	4.1	3.42	7.74 ± 0.56
$\Gamma(\eta \to \gamma\gamma)$ [eV]	215	213	460 ± 40
$\Gamma(\eta' \to \gamma\gamma)$ [eV]	2320	1480	4290 ± 150
$\Gamma(f_0(400-1200) \to \gamma\gamma)$ [eV]	—	232	10000± 6000(*)
$\Gamma(f_0(980) \to \gamma\gamma)$ [eV]	1760	—	390 ± 130
$\Gamma(a_0(980) \to \gamma\gamma)$ [eV]	—	500	300 ± 100(*)

5-point Green's function yielding

$$\langle \mathcal{M}(P') \,|\, j^\mu(0) |\, \mathcal{M}(P) \rangle = -\int \frac{\mathrm{d}^4 p}{(2\pi)^4}$$
$$\times \mathrm{tr}\Big[e_1 \bar{\Gamma}^{P'}_{(\mathcal{M})}\Big(p - \frac{q}{2}\Big) S_1^F\Big(\frac{P}{2} + p - q\Big)\gamma^\mu S_1^F\Big(\frac{P}{2} + p\Big)\Gamma^P_{(\mathcal{M})}(p)$$
$$\times S_2^F\Big(-\frac{P}{2} + p\Big) + e_2 \bar{\Gamma}^{P'}_{(\mathcal{M})}\Big(p + \frac{q}{2}\Big) S_1^F\Big(\frac{P}{2} + p\Big)\Gamma^P_{(\mathcal{M})}(p)$$
$$\times S_2^F\Big(-\frac{P}{2} + p\Big)\gamma^\mu S_2^F\Big(-\frac{P}{2} + p + q\Big)\Big], \qquad (28)$$

where the trace is understood with respect to the Dirac indices. The details of this procedure as well as a discussion of the shape of the form factor $F_\pi(Q^2)$ at very low Q^2 can be found in [5].

We show the form factor $Q^2 \cdot F_\pi(Q^2)$ in fig. 12. The correct behaviour of the form factor at very large Q^2 can be traced back to the Lorentz boost that is applied to the outgoing vertex function. The charged kaon form factor is plotted in fig. 13; we conclude that our model provides a satisfying description of the electromagnetic $\pi^\pm$ and $K^\pm$ form factors in both parameter sets. Let us finally note that the correct form factor normalization $F_\mathcal{M}(Q^2 = 0) = 1$ is a consequence of the normalization condition of the Bethe-Salpeter equation; we therefore do not need to impose an *ad hoc* normalization of the electromagnetic form factor.

4.4 The electromagnetic decay widths for $\mathcal{M} \to \mathcal{M}'\gamma$

To complete our discussion on electromagnetic processes involving mesons and to update the results of ref. [5], we will briefly comment on the widths of the decays $\mathcal{M}(P) \to \mathcal{M}'(P')\gamma(q)$. For this purpose, we extend the matrix element in eq. (28) to processes like $\rho \to \pi\gamma$ where also $J \neq 0$ mesons occur. The related decay form factor $F_{\rho\pi}(Q^2)$ with $Q^2 = -q^2$ is then given by

$$\langle \pi(P') \,|J_\mu(0)|\, \rho(P,\lambda) \rangle = \mathcal{Q} F_{\rho\pi}(Q^2) \varepsilon_{\mu\nu\alpha\beta} \frac{\epsilon_\rho^\nu(P,\lambda) P'^\alpha P^\beta}{M_\rho}. \qquad (29)$$

Here, $\epsilon_\rho(P,\lambda)$ denotes the polarization vector of the ρ meson with spin projection λ; analogue definitions hold for

all processes that will be discussed in the following. The general decay width can be computed via

$$\Gamma_{\mathcal{M}\to\mathcal{M}'\gamma} = \alpha \frac{1}{2J+1}\frac{q}{M_{\mathcal{M}}^2} \times \sum_{M_J M_{J'}} \left|\epsilon_\gamma^\mu(\vec{q},+1)\,\langle \mathcal{M}'(P',J',M_{J'})\,|J_\mu(0)|\,\mathcal{M}(P,J,M_J)\rangle\right|^2, \tag{30}$$

where ϵ_γ is the polarization vector of the photon with three-momentum $\vec{q} = q\vec{e}_z$ and the matrix element is evaluated in the rest frame of meson $\mathcal{M}$ with $P = (M, \vec{0})$.

We show the widths for various meson decays in table 8 and compare them to the latest PDG data compilation (see [19]). As already stated in [5], we clearly underestimate the processes with a pion in the final state, especially in model $\mathcal{B}$. Obviously this is again a significant shortcoming of the instantaneous approximation for deeply bound particles such as the pion; the resulting lack of retardation effects seems to spoil the correct overlapping of the associated wave functions in our calculation. Note however for the $\rho/\omega \to \pi\gamma$ decays that an exact SU(2) flavour symmetry — *i.e.* $m_u = m_d$ — implies $\Gamma_{\rho^\pm\to\pi^\pm\gamma} = \Gamma_{\rho^0\to\pi^0\gamma} = \frac{1}{9}\Gamma_{\omega^0\to\pi^0\gamma}$ as can be seen from the calculated values; therefore the results for the experimental widths in table 8 are rather puzzling.

We stress that the excellent results for $\Gamma_{\mathcal{M}\to\eta\gamma}$ with $\mathcal{M} = \rho^0, \omega, \phi$ indicate that the coefficients X_η and Y_η for the *non-strange/strange* flavour mixing are determined well in both models, see table 2. In addition, we find plausible results for the decays $\eta' \to \rho^0\gamma$ and $\eta' \to \omega\gamma$ with the calculated widths in both models close to the experimental findings.

Due to the $J = 0$ selection rule for 't Hooft's flavour-dependent interaction, no flavour mixing is induced for the ω, ϕ and f_1 mesons. It is therefore not surprising that we find vanishing decay widths for some processes since, *e.g.*, a pure *non-strange* state ($\sim n\bar{n}$) like the ω does not couple to a pure *strange* state ($\sim s\bar{s}$) like the ϕ thus yielding $\Gamma_{\phi\to\omega\gamma} = 0$ in both models; we do not quote these zero widths in table 8.

In the kaonic sector, we find a very good agreement of the $\Gamma_{K^*\to K\gamma}$ widths in model $\mathcal{A}$ with the PDG values; our numerical results in model $\mathcal{B}$ slightly underestimate the experimental data although we can describe the correct ratio between the neutral and the charged decay mode.

Let us now come back to the form factor defined in eq. (29). For the decay $\omega \to \pi^0\gamma^*$ with the virtual photon decaying into $\mu^+\mu^-$, there are some experimental values for the normalized form factor $\tilde{F}_{\omega\pi}(Q^2) = F_{\omega\pi}(Q^2)/F_{\omega\pi}(0)$ at timelike photon virtuality $q^2 = -Q^2 > 0$. In fig. 14, we have plotted these experimental data points and our numerical results, calculated with the parameters of the models $\mathcal{A}$ and $\mathcal{B}$. Note that for $Q^2 > -(m_q^2 + m_{\bar{q}}^2)$ our model will become ill-defined since we cannot guarantee confinement for timelike momentum transfers; we therefore did not compute $\tilde{F}_{\omega\pi}(Q^2)$ beyond the threshold at $\approx -0.37\,\mathrm{GeV}^2$ of model $\mathcal{A}$. Comparing our calculated curves with the experimental data and with a pole fit according to

$$\tilde{F}_{\omega\pi}(Q^2) = \frac{1}{1 + Q^2/\Lambda^2}\,, \tag{31}$$

we find that we underestimate the shape of the form factor in the timelike region; obviously, this again can be traced back to the shortcomings of our model in the case of a π meson in the final state as has been discussed above. However, our results are comparable for $Q^2 > 0$ with the pole fit extracted in the experimental study in ref. [47]. The authors found $\Lambda_{\mathrm{exp}} = (650 \pm 30)\,\mathrm{MeV}$ while our form factors would merely coincide with a simple ρ pole ansatz, *i.e.* $\Lambda_\rho \approx 770\,\mathrm{MeV}$; this discrepancy becomes obvious for $Q^2 < 0$.

Summarizing this subsection on the electromagnetic decay widths, we conclude that we find a good overall agreement with the experimental data on the level of a factor of ≈ 1.5 in the amplitudes with one exception: for a pion in the final state, our calculations fail significantly.

Table 8. The widths of the decays $\mathcal{M} \to \mathcal{M}'\gamma$, calculated with the parameters of the models $\mathcal{A}$ and $\mathcal{B}$.

Decay width	Model $\mathcal{A}$	Model $\mathcal{B}$	PDG 2000 [19]
$\Gamma(\rho^\pm \to \pi^\pm\gamma)$ [keV]	35.0	20.6	68 ± 7
$\Gamma(\rho^0 \to \pi^0\gamma)$ [keV]	35.0	20.6	102 ± 26
$\Gamma(\rho^0 \to \eta\gamma)$ [keV]	49.7	39.8	36 ± 12
$\Gamma(\omega \to \pi^0\gamma)$ [keV]	315	185	717 ± 42
$\Gamma(\omega \to \eta\gamma)$ [keV]	5.52	4.42	5.5 ± 0.8
$\Gamma(\eta' \to \rho^0\gamma)$ [keV]	87.3	28.0	60 ± 5
$\Gamma(\eta' \to \omega\gamma)$ [keV]	9.70	3.11	6.1 ± 0.8
$\Gamma(\phi \to \eta\gamma)$ [keV]	58.1	34.7	58 ± 2
$\Gamma(\phi \to \eta'\gamma)$ [keV]	0.01	0.074	0.30 ± 0.16
$\Gamma(K^{*\pm} \to K^\pm\gamma)$ [keV]	48.0	28.8	50 ± 5
$\Gamma(K^{*0} \to K^0\gamma)$ [keV]	102	70.2	116 ± 10
$\Gamma(b_1^\pm \to \pi^\pm\gamma)$ [keV]	9.21	7.05	230 ± 60
$\Gamma(f_1(1285) \to \rho^0\gamma)$ [keV]	365	208	1320 ± 310

4.5 The decays $\pi^+ \to e^+\nu_e\gamma$ and $K^+ \to e^+\nu_e\gamma$

The so-called $\pi_{\ell 2\gamma}$ decay, *i.e.* $\pi^+(P) \to \ell^+(p_\ell)\nu_\ell(p_\nu)\gamma(q)$, with the lepton $\ell = e, \mu$ and the analogously defined $K_{\ell 2\gamma}$ decay have been studied extensively both experimentally and theoretically in the last decade. For a muon in the final state, the $\pi_{\ell 2\gamma}$ decay would be dominated by Bremsstrahlung effects; however, for $\ell = e$ this contribution is strongly helicity suppressed such that the structure-dependent parts of the related amplitude can be measured.

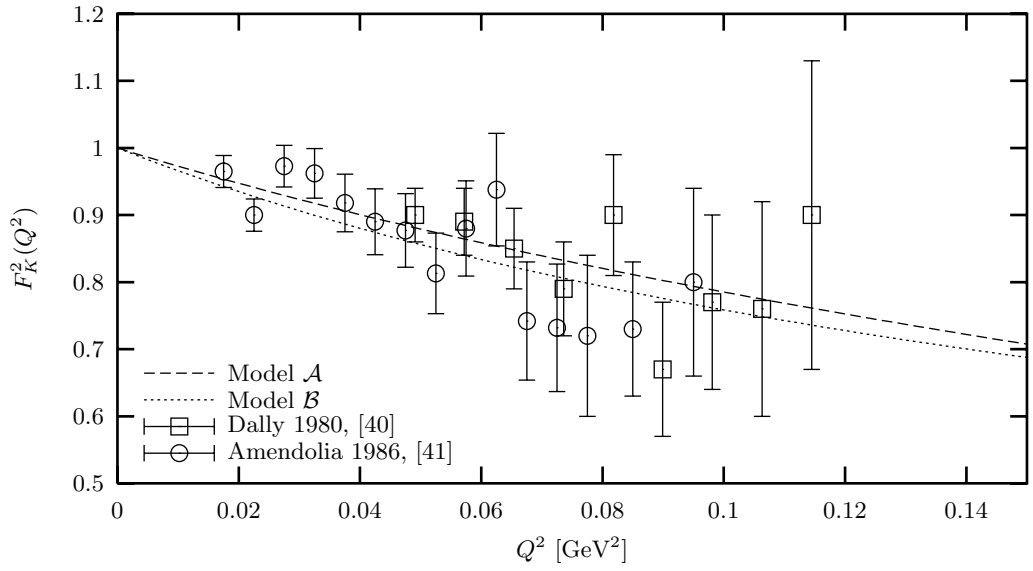

Fig. 13. The electromagnetic form factor $F_K^2(Q^2)$ of the charged kaon, calculated with the parameters of model $\mathcal{A}$ and model $\mathcal{B}$.

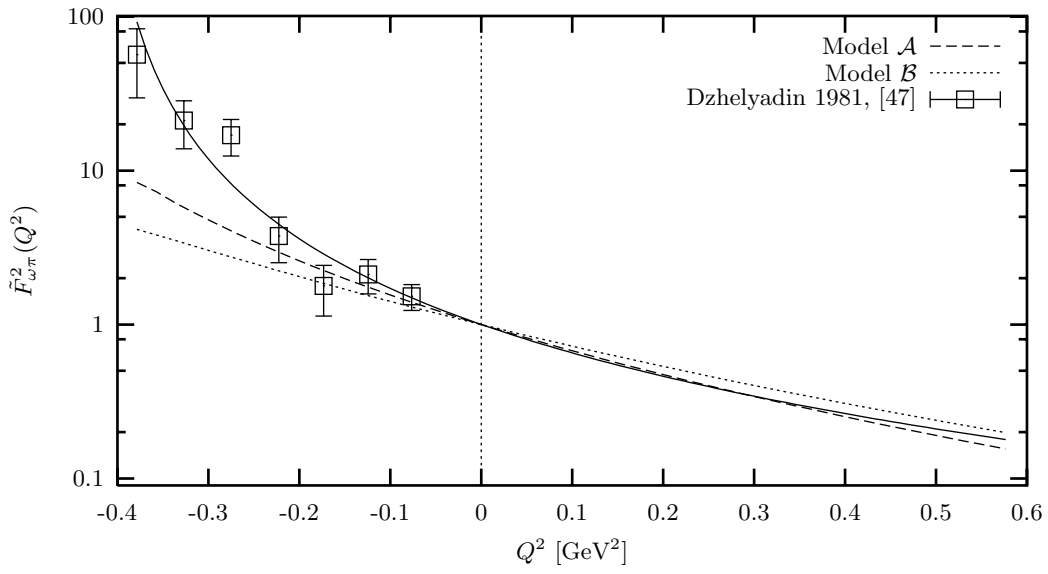

Fig. 14. The normalized decay form factor $\tilde{F}^2_{\omega\pi}(Q^2) = (F_{\omega\pi}(Q^2)/F_{\omega\pi}(0))^2$, calculated with the parameters of model $\mathcal{A}$ and model $\mathcal{B}$. The solid line is the pole fit of ref. [47] with the parameter $\Lambda = 0.65\,\mathrm{GeV}$, see eq. (31).

The matrix element for this process reads

$$\mathcal{M}_{\pi^+\to e^+\nu_e\gamma} = -\frac{eG_F}{\sqrt{2}} V_{ud}^* \varepsilon^{\mu *}(q) M_{\mu\nu}^{\ell 2\gamma}(p,q) \bar{u}(p_\nu)\gamma^\nu(\mathbb{1}+\gamma_5)v(p_e)\ , \quad (32)$$

where $\bar{u}(p_\nu)$ and $v(p_e)$ denote the Dirac spinors for the neutrino and the positron (see [42,43] and the PDG mini-review in [19]). Here, the outgoing photon is real so that for its polarization vector $\varepsilon \cdot q = 0$ with $q^2 = 0$ holds. The quantity $M_{\mu\nu}^{\ell 2\gamma}$ can be formulated as the time-ordered product of the electromagnetic current $J_\mu^{\text{el.magn.}}$ and the weak current J_ν^{weak} and reads explicitly:

$$\begin{aligned} M_{\mu\nu}^{\ell 2\gamma}(p,q) &= \int \mathrm{d}^4x \ \left\langle 0 \left| J_\mu^{\text{el.magn.}}(x) J_\nu^{\text{weak}}(0) \right| \pi^+(P) \right\rangle e^{iq\cdot x} \\ &= f_\pi \left(g_{\mu\nu} - \left\langle \pi^+(P-q) \left| J_\mu^{\text{el.magn.}} \right| \pi^+(P) \right\rangle \frac{(P-q)_\nu}{(P-q)^2 - M_\pi^2} \right) \\ &\quad - h_A \left((P-q)_\mu\, q_\nu - q\cdot(P-q)\, g_{\mu\nu} \right) + i h_V \epsilon_{\mu\nu\alpha\beta} q^\alpha P^\beta \ . \quad (33) \end{aligned}$$

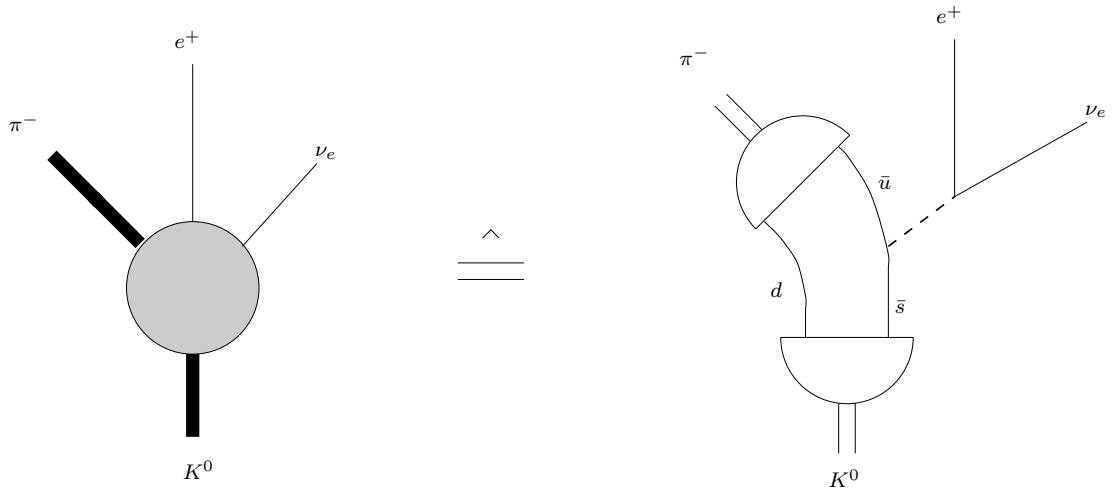

Fig. 15. The decay $K^0 \to \pi^- \ell^+ \nu_\ell$ in lowest order in the Mandelstam formalism.

Table 9. The form factors of the $\pi_{\ell 2\gamma}$ decay and the $K_{\ell 2\gamma}$ decay, calculated with the parameters of the models $\mathcal{A}$ and $\mathcal{B}$.

Decay mode	Form factor	Model $\mathcal{A}$	Model $\mathcal{B}$	PDG 2000 [19]
$\pi_{\ell 2\gamma}$	h_V	0.014	0.017	0.017 ± 0.008
	h_A	0.012	0.010	0.0116 ± 0.0016
$K_{\ell 2\gamma}$	$h_A + h_V$	0.124	0.117	0.148 ± 0.010
	$h_A - h_V$	-0.042	-0.051	$-2.2 \ldots + 0.3$

The first term including f_π is the so-called Born part; the subscripts at the form factors h_V and h_A denote their origin either in the vector (V) or in the axial vector (A) part of the weak current. Note that an additional axial form factor occurs if the outgoing photon is virtual, *i.e.* for the decays $\pi^+/K^+ \to e^+\nu_e e^+ e^-$; we will not study these processes here.

In eq. (33), the Born terms contain the pion form factor; this quantity has been calculated in the framework of our model, see the foregoing subsection. As it stands, the full matrix element is gauge invariant due to the inclusion of the Born terms. In the following, we will only consider the structure-dependent contributions, but we will take care that in the extraction of the form factors from the full tensor $M^{\ell 2\gamma}_{\mu\nu}$ no terms will occur that violate gauge invariance.

The structure-dependent parts of eq. (33) can be calculated in the Mandelstam formalism. The result is analogous to the matrix element of the two-photon decay, see eq. (19) and fig. 8 except that one photon line is substituted by a W^+ boson line with the typical $V - A$ Dirac structure and the flavour matrix $\lambda_1 - i\lambda_2$. The calculation can be extended to the $K_{\ell 2\gamma}$ decays by inserting kaon observables M_K, F_K in eq. (33) and by using the corresponding matrix in flavour space.

In table 9, we present the results for the form factors h_V and h_A of the $\pi_{\ell 2\gamma}$ decay as well as for the $K_{\ell 2\gamma}$ decay. They are compared with the world averages of the Particle Data Group (see [19]). The form factors of the $K_{\ell 2\gamma}$ decay are known only incompletely; we quote the experimental results for the sum and the difference of h_V and h_A. In the case of the $\pi_{e2\gamma}$ decay, one has to regard the values of the axial form factor h_A with care. Since usually only the ratio $\gamma := h_A/h_V$ is measured and only two direct determinations of h_V are presented up to now, the PDG results for h_A are determined via this ratio with the input $h_V^{\rm CVC} = (0.0259 \pm 0.0005)/M_\pi^2$ from the CVC prediction. Despite this caveat, we will however quote the results of ref. [19] for a comparison of our results with experimental data. We obtain excellent results compared to the PDG averages in both models, see table 9.

4.6 Form factors of the $K_{\ell 3}$ decay

The processes $K^+ \to \pi^0 \ell^+ \nu_\ell$ and $K^0 \to \pi^- \ell^+ \nu_\ell$ are called $K^+_{\ell 3}$ and $K^0_{\ell 3}$ decay, respectively. They are usually parameterized in terms of two form factors for which isospin invariance requires $f_\pm^{K^+\pi^0} = f_\pm^{K^0\pi^-}/\sqrt{2} =: f_\pm$ (see the minireview in [19]):

$$\begin{aligned}\left\langle \pi^0(P') \middle| J_\mu^{\rm weak} \middle| K^+(P) \right\rangle &= f_+^{K^+\pi^0}(P+P')_\mu + f_-^{K^+\pi^0}(P-P')_\mu\,,\\ \left\langle \pi^-(P') \middle| J_\mu^{\rm weak} \middle| K^0(P) \right\rangle &= f_+^{K^0\pi^-}(P+P')_\mu + f_-^{K^0\pi^-}(P-P')_\mu.\end{aligned} \tag{34}$$

In fig. 15, we show the $K^0_{\ell 3}$ decay in our Bethe-Salpeter quark model picture. Note that we describe the emission of the leptonic pair by a W^+ boson coupling to the *strange* quark and decaying into $\ell^+\nu_\ell$.

For heavy quark systems, semileptonic decays of this type can also be calculated in our model if either an additional one-gluon exchange potential (see [7]) or an appropriate extension of 't Hooft instanton-induced force is

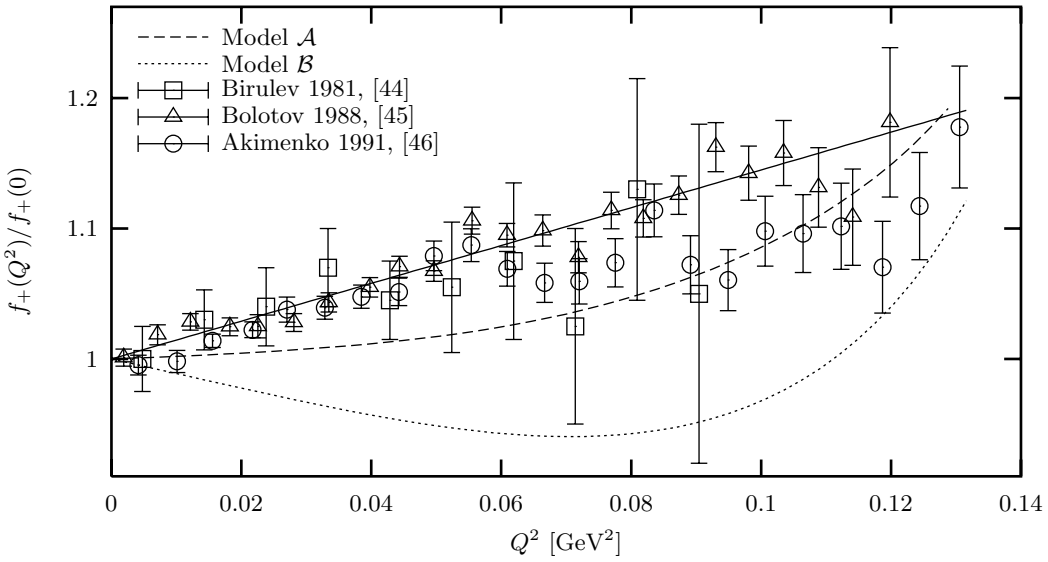

Fig. 16. The normalized form factor $f_+(Q^2)/f_+(0)$ of the $K_{\ell 3}$ decay, calculated with the parameters of model $\mathcal{A}$ and model $\mathcal{B}$. The solid line indicates the linear fit according to eq. (36) with the parameter $\lambda_+^{\mathrm{PDG}} = (0.0276 \pm 0.0021)/M_\pi^2$, see ref. [19].

Table 10. The form factors of the $K_{\ell 3}$ decay and their ratio ξ at $Q^2 = 0$, calculated with the parameters of the models $\mathcal{A}$ and $\mathcal{B}$.

Form factor	Model $\mathcal{A}$	Model $\mathcal{B}$	PDG 2000 [19]
$f_+(0)$	-0.813	-0.803	—
$f_-(0)$	0.121	0.154	—
$\xi(0)$	-0.148	-0.192	-0.31 ± 0.15

adopted; a subsequent paper on this subject is currently in preparation.

The matrix element for the $K_{\ell 3}$ decay can be defined analogously to the expression for the electromagnetic form factor of the $\pi^\pm/K^\pm$ meson, see eq. (28). In our model, it reads explicitly

$$\begin{aligned}\left\langle \pi^-(P') \left| J_\mu^{\mathrm{weak}} \right| K^0(P) \right\rangle = &- \int \frac{\mathrm{d}^4 p}{(2\pi)^4} \\ &\times \mathrm{tr} \left[\bar{\Gamma}^{P'}_{(\pi^-)} \left(p + \frac{q}{2} \right) S_d^F \left(\frac{P}{2} + p \right) \Gamma^P_{(K^0)}(p) \right. \\ &\left. \times S_{\bar{s}}^F \left(-\frac{P}{2} + p \right) \bar{u} \gamma_\mu s S_{\bar{u}}^F \left(-\frac{P}{2} + p + q \right) \right] . \quad (35)\end{aligned}$$

Note that for $0^- \to 0^-$ transitions only the vector part of the weak coupling in $J_\mu^{\mathrm{weak}} \,|_{\mathrm{Dirac}} = \gamma_\mu(\mathbb{1} - \gamma_5)$ contributes to the form factors; furthermore, a second term with a W boson coupling to the d quark trivially does not occur due to its vanishing flavour trace.

In most experiments, the $q^2 = (P' - P)^2 =: -Q^2$ dependence of the $f_\pm$ form factor is found to be consistent with a linear parametrization like

$$f_\pm(Q^2) = f_\pm(0) \, \left(1 + \lambda_\pm \cdot Q^2 \right) . \quad (36)$$

Since f_- is multiplied by the lepton mass, this form factor is difficult to measure; however, there exist some rough experimental values for the ratio $\xi := f_-/f_+$.

In table 10, we show our results for the form factors at $Q^2 = 0$ and their ratio ξ. For f_+ and f_-, the absolute values of these form factors are not determined so that only their ratio can be compared with experimental estimations.

We show the Q^2 dependence of the normalized f_+ form factor in fig. 16. Obviously, a linear fit to the experimental data is justified only approximately; indeed, our results show remarkable non-linear shapes. Although the data are underestimated in model $\mathcal{B}$, they can be acceptably described with the parameters of model $\mathcal{A}$ so that no general shortcoming of our model can be stated.

Let us finally note a special feature of our model: the *non-strange* and the *strange* quark sector are distinct not only due to different constituent masses, but also because of the 't Hooft couplings g and g'. In the simultaneous limit $m_s \to m_n$ and $g' \to g$, the $SU_F(3)$ symmetry is restored and thus the kaon amplitude will become the pion amplitude. The $SU_F(3)$ limit leads then to $-f_+(Q^2) \to F_\pi(Q^2)$ and $f_-(Q^2) \to 0$ with $F_\pi(Q^2)$ being the well-known pion form factor, see eq. (27); this trivial result has been checked numerically in our model.

5 Summary and outlook

In this paper, we have presented some new results of a relativistic quark model for mesons. We have briefly resumed our approach on the basis of the Bethe-Salpeter equation in its instantaneous approximation. The potential in the resulting three-dimensional reduction is a combination of a linear confinement potential plus a residual interaction *à la* 't Hooft based on instanton effects.

Our numerical calculations were done with two different parameter sets that have distinct Dirac structures for the confinement. The discussion of the complete meson spectrum shows an excellent agreement with the experimental data; the correct splittings in the pseudoscalar sector can be backtraced to the effects of our residual interaction which in turn yields remarkable splittings for scalar states. We found considerable differences between the spectra of model $\mathcal{A}$ and model $\mathcal{B}$: the masses of all $J^\pi = 0^+$ ground states were significantly lowered in model $\mathcal{B}$ so that the assignment of possible $q\bar{q}$ states in this puzzling sector will differ in both models.

Furthermore, we have investigated various meson decay modes such as the $K_{\ell 3}$ decay and $\pi^0, \eta, \eta' \to \gamma\gamma$. The latter transitions were studied not only for real photons but also for very high virtualities. We found that our model fails if only one photon is virtual: the asymptotic limit (*e.g.*, $Q^2 F_{\gamma\gamma}^{\pi^0}(Q^2, 0) \to 2 f_{\pi^0}$) known from perturbative QCD is not recovered. However, we can proof similar relations for $Q^2 F_{\gamma\gamma}^{\mathcal{M}}(Q^2, Q^2)$ linking the transition form factor of the meson $\mathcal{M} = \pi^0, \eta, \eta'$ to its decay constants in the case of symmetric photon virtualities. We stress that the analytic calculations presented here are in fact model-independent. Finally, we found excellent agreement of the various form factors in the decays $\pi^+/K^+ \to \ell^+ \nu_\ell \gamma$ as well as a satisfying description of the electromagnetic $\pi^\pm/K^\pm$ form factors in both parameter sets.

The relativistic quark model presented in this paper also allows further investigations; we have already mentioned an extension of 't Hooft's residual interaction for heavy $q\bar{q}$ systems. A further topic is the study of strong decays in this framework. Hereby, it is of special interest that not only pure quark loops contribute to the strong decay widths, but also instanton-induced six-quark interactions will occur. Furthermore, we have studied the various implications of our quark model with respect to the concept of spontaneous breaking of the chiral symmetry; various low-energy theorems can be tested and compared with results from Chiral Perturbation Theory. A last point to mention is the study of Compton scattering off a pseudoscalar meson: it is possible to calculate the corresponding matrix elements in the framework of our Bethe-Salpeter model and compute the electromagnetic polarizabilities, even in their generalized form for virtual photons. All these various aspects are currently prepared for publication and will soon be presented in subsequent papers.

We thank E. Klempt, V.V. Anisovich and A. Sarantsev for fruitful discussions. Financial support of the Deutsche Forschungsgemeinschaft (DFG) is gratefully acknowledged.

Appendix A.

In this Appendix, we present a model-independent factorization proof for the asymptotic limit ($Q^2 \to \infty$) of the pseudoscalar transition form factor $Q^2 F_{\gamma\gamma}^{\mathcal{M}}(Q^2, Q^2)$ at equal photon virtualities. We stress that the following considerations are formulated on the basis of full four-dimensional Bethe-Salpeter amplitudes and quark propagators so that they will be independent of the instantaneous approximation that we adopted for our numerical evaluations.

Let us start with the matrix element $T_{\gamma\gamma}^{\mathcal{M}}$ in eq. (19) for the decays $\mathcal{M} \to \gamma\gamma$ with $\mathcal{M} = \pi^0, \eta, \eta'$ at arbitrary photon virtualities $Q_i^2 = -q_i^2$. We define $q := \frac{1}{2}(q_1 - q_2)$ and consider the decaying meson in its rest frame with $P = (M, \vec{0})$. With $q_1 = P/2 + q$ and $q_2 = P/2 - q$, we then find the following relations for $Q_1^2 = Q_2^2 =: Q^2 \to \infty$:

$$\begin{array}{l} q^2 \to -Q^2 \\ q^0 \to \ \ 0 \end{array} \implies \begin{array}{l} q_1^0, q_2^0 \ \to \ \ \frac{M}{2} \\ q_1^3, -q_2^3 \to \sqrt{Q^2}\,. \end{array} \tag{A.1}$$

Here, we have chosen the photon momenta to be in the direction of the z-axis. We now study the behaviour of the intermediate propagator in both terms of the matrix element $T_{\gamma\gamma}^{\mathcal{M}}$ in eq. (19). The denominator behaves like $(P/2 + p - q_i)^2 \to -Q^2$ for asymptotic photon virtualities since terms proportional to the relative momentum p will not contribute due to the vanishing vertex function for $p \to \infty$. For the same reason, only a $\vec{q}_i \vec{\gamma} = \pm\sqrt{Q^2}\gamma^3$ term survives in the numerator ("+" for $i = 1$, "−" for $i = 2$). Therefore we find for the complete intermediate quark propagator

$$S^F\left(\frac{P}{2} + p + q_i\right) \to \pm \frac{\sqrt{Q^2}}{Q^2}\gamma_3 \qquad \text{as} \quad Q^2 \to \infty\,. \tag{A.2}$$

Inserting this in the matrix element of eq. (19), we find

$$\begin{aligned} T_{\gamma\gamma}^{\mathcal{M}} \to & -i\sqrt{3}\,\frac{\sqrt{Q^2}}{Q^2}\int \frac{\mathrm{d}^4 p}{(2\pi)^4} \\ & \times \mathrm{tr}\left[S^F\!\left(\frac{P}{2}+p\right)\Gamma_{(\mathcal{M})}^P(p) S^F\!\left(-\frac{P}{2}+p\right)\left(\not{\varepsilon}_2\gamma_3\ \not{\varepsilon}_1 - \not{\varepsilon}_1\gamma_3\ \not{\varepsilon}_2\right)\right] \end{aligned} \tag{A.3}$$

for asymptotic virtualities. Since we are dealing with virtual photons, the polarization vectors $\varepsilon_i = (0, \vec{\varepsilon}_i)$ do not only have transversal but also longitudinal components. However, if one of the photons is longitudinally polarized with $\vec{\varepsilon}_i \parallel \vec{q}_i \parallel \vec{e}_3$, the two terms in eq. (A.3) will cancel. The same happens for $\vec{\varepsilon}_1 = \vec{\varepsilon}_2$ so that we conclude

$$\not{\varepsilon}_2\gamma_3\ \not{\varepsilon}_1 - \not{\varepsilon}_1\gamma_3\ \not{\varepsilon}_2 = \begin{cases} 0, & \text{if} \quad \vec{\varepsilon}_1 = \vec{\varepsilon}_2 \ \text{ or } \vec{\varepsilon}_i \parallel \vec{q}_i \\ \mp 2i\gamma_0\gamma_5, & \text{otherwise,} \end{cases} \tag{A.4}$$

where, as usual, $\gamma_5 = i\gamma_0\gamma_1\gamma_2\gamma_3$. Here and in the following, the upper sign ("−") stands for polarization vectors $\varepsilon_1 = (0, 1, 0, 0)$ and $\varepsilon_2 = (0, 0, 1, 0)$, while the lower sign ("+") applies to the choice $\varepsilon_1 = (0, 0, 1, 0)$ and $\varepsilon_2 = (0, 1, 0, 0)$. The resulting integrand is equivalent to the expression for the pseudoscalar decay constants in eq. (15) in its four-dimensional generalization for $\mathcal{M} = \pi^0, \eta, \eta'$. By comparison of the asymptotic matrix element and the definition of the decay constants $f_{\mathcal{M}}^j$ ($j = \pi, n, s$) we find

$$T^{\mathcal{M}}_{\gamma\gamma} \to \mp 2\sqrt{3}\,\frac{\sqrt{Q^2}}{Q^2}\int\frac{\mathrm{d}^4p}{(2\pi)^4} \times \mathrm{tr}\left[S^F\left(\frac{P}{2}+p\right)\Gamma^P_{(\mathcal{M})}(p)S^F\left(-\frac{P}{2}+p\right)\gamma_0\gamma_5\right] = \mp 2\frac{M_{\mathcal{M}}\sqrt{Q^2}}{Q^2}\sum_j \tilde{C}_j f^j_{\mathcal{M}}\,, \quad \text{(A.5)}$$

as $Q^2 \to \infty$. If we consider the process $\pi^0 \to \gamma\gamma$, the sum becomes trivial and contains only the pion decay constant f_π multiplied by the factor $\tilde{C}_\pi = \alpha/(3\sqrt{2})$. We note that we have introduced the charge factors $\tilde{C}_j := \alpha C_j$ that are proportional to the factors defined in sect. 4.2. Now we recall the relation between the matrix element of the two photon decay and the transition form factor in eq. (20). Since we have set the photon momenta as $q_i = (q_i^0; 0, 0, q_i^3)$, we can evaluate the implicit sum over the indices μ, ν, α and β. This yields

$$\mp\alpha M_{\mathcal{M}}\sqrt{Q^2}F^{\mathcal{M}}_{\gamma\gamma}(Q^2,Q^2) = \mp 2\frac{M_{\mathcal{M}}\sqrt{Q^2}}{Q^2}\sum_j \tilde{C}_j f^j_{\mathcal{M}} \quad \text{as} \quad Q^2 \to \infty\,, \quad \text{(A.6)}$$

so that we finally arrive at the asymptotic limits quoted in eqs. (25) and (26):

$$\lim_{Q^2\to\infty} Q^2 F^{\pi^0}_{\gamma\gamma}(Q^2,Q^2) = \frac{2}{3}f_{\pi^0}\,, \quad \text{(A.7)}$$

$$\lim_{Q^2\to\infty} Q^2 F^{\eta}_{\gamma\gamma}(Q^2,Q^2) = \frac{5}{9\sqrt{2}}f^n_\eta + \frac{1}{9}f^s_\eta\,, \quad \text{(A.8)}$$

$$\lim_{Q^2\to\infty} Q^2 F^{\eta'}_{\gamma\gamma}(Q^2,Q^2) = \frac{5}{9\sqrt{2}}f^n_{\eta'} + \frac{1}{9}f^s_{\eta'}\,. \quad \text{(A.9)}$$

We want to emphasize that this proof is entirely model-independent since we only explored kinematical properties of the diagrams in fig. 8 without making any assumptions on the meson vertex function, in particular without applying the instantaneous approximation.

References

1. S. Godfrey, N. Isgur, Phys. Rev. D **32**, 189 (1985).
2. C.R. Münz, J. Resag, B.C. Metsch, H.R. Petry, Nucl. Phys. A **578**, 397 (1994).
3. C.R. Münz, J. Resag, B.C. Metsch, H.R. Petry, Nucl. Phys. A **578**, 418 (1994).
4. J. Resag, C.R. Münz, Nucl. Phys. A **590**, 735 (1995).
5. C.R. Münz, J. Resag, B.C. Metsch, H.R. Petry, Phys. Rev. C **52**, 2110 (1995).
6. E. Klempt, B.C. Metsch, C.R. Münz, H.R. Petry, Phys. Lett. B **361**, 160 (1995).
7. G. Zoller, S. Hainzl, C.R. Münz, M. Beyer, Z. Phys. C **68**, 103 (1995).
8. C. Ritter, B.C. Metsch, C.R. Münz, H.R. Petry, Phys. Lett. B **380**, 431 (1996).
9. C.R. Münz, Nucl. Phys. A **609**, 364 (1996).
10. W.I. Giersche, C.R. Münz, Phys. Rev. C **53**, 2554 (1996).
11. E.E. Salpeter, H.A. Bethe, Phys. Rev. **84**, 1232 (1951).
12. E.E. Salpeter, Phys. Rev. **87**, 328 (1952).
13. G. 't Hooft, Phys. Rev. D **14**, 3432 (1976).
14. M. Böhm, H. Joos, M. Krammer, Nucl. Phys. B **51**, 397 (1973).
15. F. Gross, J. Milana, Phys. Rev. D **43**, 2401 (1991).
16. R. Ricken, D. Merten, M. Koll, B.C. Metsch, H.R. Petry, *The Meson Spectrum in a Covariant Quark Model*, to be published in Eur. Phys. J. A **9** (2000).
17. R. Ricken, D. Merten, M. Koll, B.C. Metsch, H.R. Petry, *Strong Decays of Light Mesons in a Covariant Quark Model* (in preparation).
18. S. Mandelstam, Proc. Roy. Soc. **233**, 248 (1955).
19. Particle Data Group, D.E. Groom et al., Eur. Phys. J. C **15**, 1 (2000).
20. V.V. Anisovich, *The lightest scalar glueball: retrospective view and the current state of the problem*, in *Hadron Spectroscopy, VIIth International Conference, Upton, NY*, AIP Conf. Proc. **432**, 421 (1997); see also: V. V. Anisovich, Phys. Usp. **41**, 419 (1998); Usp. Fiz. Nauk **168**, 481 (1998).
21. J.-S. Suh, *Observation of the $\eta(1440)$ in the reaction $p\bar{p} \to \pi^+\pi^-\pi^+\pi^-\eta$*, in *Frascati Physics Series*, Vol. XV, 555 (1999); see also: J.-S. Suh, Nucl. Phys. A **675**, 100c (2000); Nucl. Phys. A **675**, 104c (2000).
22. T. Feldmann, P. Kroll, B. Stech, Phys. Rev. D **58**, 114006 (1998).
23. T. Feldmann, P. Kroll, B. Stech, Phys. Lett. B **449**, 339 (1999).
24. F.-G. Cao, A.I. Signal, Phys. Rev. D **60**, 114012 (1999).
25. A. Seiden, H.F.W. Sadrozinski, H.E. Haber, Phys. Rev. D **38**, 824 (1988).
26. A. Falvard et al., *DM2 results on J, ψ and η_c decays*, in *Proceedings of the International Europhysics Conference on High Energy Physics, Uppsala*, Vol. I, 539 (1987).
27. S.J. Brodsky, G.P. Lepage, Phys. Rev. D **24**, 1808 (1981).
28. S.J. Brodsky, C.-R. Ji, A. Pang, D.G. Robertson, Phys. Rev. D **57**, 245 (1998).
29. T. Feldmann, P. Kroll, Phys. Rev. D **58**, 057501 (1998).
30. TPC, Two-Gamma Collaboration, Phys. Rev. Lett. **64**, 172 (1990).
31. Cello Collaboration, Z. Phys. C **49**, 401 (1991).
32. L3 Collaboration, CERN-PPE, 97-110 (1997); Phys. Lett. B **418**, 399 (1998).
33. Cleo Collaboration, Phys. Rev. D **57**, 33 (1998).
34. V.A. Novikov, M.A. Shifman, A.I. Vainshtain, M.B. Voloshin, V.I. Zakharov, Nucl. Phys. B, **237**, 525 (1984).
35. A. Anselm, A. Johansen, E. Leader, L. Lukaszuk, Z. Phys. A **359**, 457 (1997).
36. C.N. Brown et al., Phys. Rev. D **8**, 92 (1973).
37. C.J. Bebek et al., Phys. Rev. D **13**, 25 (1976); C.J. Bebek et al., Phys. Rev. Lett. **37**, 1525 (1976).
38. C.J. Bebek et al., Phys. Rev. D **17**, 1693 (1978).
39. S.R. Amendolia et al., Nucl. Phys. B **277**, 168 (1986).
40. E.B. Dally et al., Phys. Rev. Lett. **45**, 232 (1980).
41. S.R. Amendolia et al., Phys. Lett. B **178**, 435 (1986).
42. D.A. Bryman et al., Phys. Rep. **88**, 151 (1982).
43. J.F. Donoghue, B.R. Holstein, Phys. Rev. D **40**, 2378 (1989); see also J.F. Donoghue, E. Golowich, B.R. Holstein, *Dynamics of the standard model*, Cambridge Monographies on Particle Physics, Nuclear Physics and Cosmology, Vol. II, Ch. VI-3 (Cambridge, 1992).
44. V.K. Birulev et al., Nucl. Phys. B **182**, 1 (1981).
45. V.N. Bolotov et al., JETP Lett. **47**, 7 (1988).
46. S.A. Akimenko et al., Phys. Lett. B **259**, 225 (1991).
47. R.I. Dzhelyadin et al., Phys. Lett. B **102**, 296 (1981).